Monthly Notices
of the
ROYAL ASTRONOMICAL SOCIETY

MNRAS **496,** 4654–4673 (2020)
Advance Access publication 2020 July 2

doi:10.1093/mnras/staa1868

# The ram pressure stripped radio tails of galaxies in the Coma cluster

Hao Chen,[1,2★] Ming Sun,[1★] Masafumi Yagi,[3,4] Hector Bravo-Alfaro,[5] Elias Brinks,[6] Jeffrey Kenney,[7] Francoise Combes,[8] Suresh Sivanandam,[9,10] Pavel Jachym,[11] Matteo Fossati,[12,13] Giuseppe Gavazzi,[14] Alessandro Boselli,[15] Paul Nulsen,[16,17] Craig Sarazin,[18] Chong Ge,[1] Michitoshi Yoshida[19,20] and Elke Roediger[21]

*Affiliations are listed at the end of the paper*

Accepted 2020 June 21. Received 2020 June 21; in original form 2019 August 8

## ABSTRACT

Previous studies have revealed a population of galaxies in galaxy clusters with ram pressure stripped (RPS) tails of gas and embedded young stars. We observed 1.4 GHz continuum and H I emission with the Very Large Array in its B-configuration in two fields of the Coma cluster to study the radio properties of RPS galaxies. The best continuum sensitivities in the two fields are 6 and 8 μJy per 4 arcsec beam, respectively, which are 4 and 3 times deeper than those previously published. Radio continuum tails are found in 10 (8 are new) out of 20 RPS galaxies, unambiguously revealing the presence of relativistic electrons and magnetic fields in the stripped tails. Our results also hint that the tail has a steeper spectrum than the galaxy. The 1.4 GHz continuum in the tails is enhanced relative to their H $\alpha$ emission by a factor of ∼7 compared to the main bodies of the RPS galaxies. The 1.4 GHz continuum of the RPS galaxies is also enhanced relative to their infrared emission by a factor of ∼2 compared to star-forming galaxies. The enhancement is likely related to ram pressure and turbulence in the tail. We furthermore present H I detections in three RPS galaxies and upper limits for the other RPS galaxies. The cold gas in D100's stripped tail is dominated by molecular gas, which is likely a consequence of the high ambient pressure. No evidence of radio emission associated with ultra-diffuse galaxies is found in our data.

**Key words:** galaxies: clusters: individual: Coma – galaxies: interactions – galaxies: ISM – radio continuum: galaxies.

## 1 INTRODUCTION

Ram pressure stripped (RPS) galaxies are characterized by gas being stripped from the affected galaxy by the intracluster medium (ICM; e.g. Gunn & Gott 1972; Nulsen 1982). Star formation (SF) can be triggered by ram pressure at the early interaction stage by compression of interstellar medium (ISM), as shown in observations and simulations (e.g. Koopmann & Kenney 2004; Crowl et al. 2006). Then, as the cold ISM is depleted, the galactic SF will be quenched (e.g. Quilis, Moore & Bower 2000; Boselli et al. 2016b). Thus, ram pressure stripping is an important process affecting galaxy evolution in rich environments like galaxy groups and clusters. The evolution of the stripped ISM is a significant area of research. The mixing of the stripped cold ISM with the hot ICM will produce a multiphase gas (e.g. Sun, Donahue & Voit 2007; Ferland et al. 2009; Jáchym et al. 2019). Some of the stripped ISM can turn into stars in the galactic halo and the intracluster space (e.g. Cortese et al. 2007; Sun et al. 2007; Owers et al. 2012; Ebeling, Stephenson & Edge 2014; Cramer et al. 2019), especially in the high ICM pressure environment (e.g. Sun et al. 2010). Thus, stripped tails emerge as ideal targets to study this multiphase medium and SF conditions in an extreme environment.

RPS tails are observed in X-rays (e.g. Sun et al. 2006, 2010; Zhang et al. 2013), far-ultraviolet (FUV; e.g. Boissier et al. 2012), H $\alpha$ (e.g. Gavazzi et al. 2001, 2017, 2018; Sun et al. 2007; Yagi et al. 2007, 2017; Yoshida et al. 2008, 2012; Smith et al. 2010; Yagi et al. 2010, 2013; Fossati et al. 2012, 2016, 2018; Fumagalli et al. 2014; Boselli et al. 2016a, 2018; Bellhouse et al. 2017), warm $H_2$ (e.g. Sivanandam, Rieke & Rieke 2010, 2014), CO (e.g. Jáchym et al. 2013, 2014, 2017; Scott et al. 2013, 2015; Verdugo et al. 2015; Moretti et al. 2018), and H I (e.g. Kenney, van Gorkom & Vollmer 2004; Oosterloo & van Gorkom 2005; Chung et al. 2007, 2009; Scott et al. 2010, 2012; Abramson & Kenney 2014; Kenney et al. 2014; Ramatsoku et al. 2019; Serra et al. 2019; Deb et al. 2020). Extensive simulations (e.g. Quilis et al. 2000; Roediger & Brüggen 2008; Ruszkowski 2012) show that stripping has a significant impact on galaxy evolution (e.g. disc truncation, the formation of flocculent arms, the transformation of dwarf galaxies). SF in the stripped tail has also been seen in simulations (e.g. Kapferer et al. 2009; Tonnesen & Bryan 2010, 2012; Roediger et al. 2014).

A complementary tool for studying stripped tails is the radio continuum emission. At 1.4 GHz, radio continuum emission is dominated by synchrotron radiation that is emitted by the relativistic electrons moving within a magnetic field. Like the colder, denser (traced by H I) and hotter, more diffuse (traced by H $\alpha$ and X-ray) gas, the plasma containing relativistic electrons and magnetic fields is stripped by ram pressure (e.g. Gavazzi & Jaffe 1987). Murphy et al. (2009) identified radio-deficit regions along the outer edge of six Virgo Cluster galaxies, revealing that relativistic electrons and magnetic fields on their leading edges had been removed by ram pressure. Furthermore, the stripped relativistic electrons can be re-

---

★ E-mail: HaoChen.cluster@gmail.com (HC); ming.sun@uah.edu (MS)

Published by Oxford University Press on behalf of the Royal Astronomical Society

accelerated (rejuvenated) in the tail (Pinzke, Oh & Pfrommer 2013), either by turbulence and ICM shocks (Kang & Ryu 2011), or by new SNe. At the same time, local core-collapse supernovae can contribute to the relativistic electrons since H II regions (tracing massive stars) have been found in RPS tails (e.g. Sun et al. 2007; Yagi et al. 2010). However, fewer tails have been detected in radio continuum than in H $\alpha$ and X-ray. For example, there are 17 stripped tails detected in H $\alpha$ in the Coma cluster (Gavazzi et al. 2018), but only 2 of them have thus far been detected in radio continuum (Miller, Hornschemeier & Mobasher 2009). Currently most of the stripped tails seen in late-type galaxies in radio continuum are short and are detected in nearby clusters, for example NGC 4522 (Vollmer et al. 2004), NGC 4402 (Crowl et al. 2005), and others in the Virgo cluster. A few long RPS tails, such as CGCG 097−073, CGCG 097−079, and UGC 6697 have been reported in Abell 1367 (Gavazzi 1978; Gavazzi & Jaffe 1985, 1987; Gavazzi et al. 1995).

Why do RPS tails tend not to be detected in the radio continuum? How common are radio continuum tails behind RPS galaxies? How does the radio continuum emission in tails correlate with emission in other bands? Are the observed radio continuum tails mainly related to SF in the tails or due to relativistic electrons that were stripped from the galaxy by ram pressure? To address these questions deep radio continuum data are needed, something that has become feasible with the new generation wide-band correlators deployed on existing radio telescopes.

As ram pressure stripping and SF activity in the tails are believed to be more prominent in high-pressure environments than in low-pressure environments (e.g. Sun et al. 2010; Tonnesen, Bryan & Chen 2011; Poggianti et al. 2016, 2017), the Coma cluster, as the most massive cluster at $z < 0.025$, is an ideal target for these studies. Coma has the richest optical data among nearby massive clusters, already with a sample of over 20 late-type galaxies with one-sided SF or ionized gas tails (Smith et al. 2010; Yagi et al. 2010; Kenney et al. 2015; Gavazzi et al. 2018). There has been an increasing effort to obtain multiwavelength observations of these galaxies. RPS tails in bands other than H $\alpha$ have been detected. A spectacular example is D100, with a narrow tail observed in X-rays with *Chandra* (Sanders et al. 2014) as well as CO detected at sub-mm wavelengths (Jáchym et al. 2017), co-existing with the narrow H $\alpha$ tail (Yagi et al. 2007).

The deepest H I data on the Coma cluster to date are those of Bravo-Alfaro et al. (2000, 2001), obtained with the VLA in its C-configuration. The angular resolution of ∼30 arcsec is not sufficient, though, for detailed study of the H I features in the galaxies and some of the narrow H $\alpha$ tails (e.g. D100's with a width of ∼4 arcsec). The deepest radio 1.4 GHz continuum data on the Coma cluster were presented in Miller et al. (2009), before the implementation of the far more powerful WIDAR correlator. In this paper, we present new H I (with higher spatial resolution) and 1.4 GHz continuum (with deeper sensitivity) data on 20 RPS galaxies in the Coma cluster.

We assume $H_0 = 70\ \mathrm{km\,s^{-1}\,Mpc^{-1}}$, $\Omega_\mathrm{m} = 0.3$, and $\Omega_\Lambda = 0.7$. At the redshift of the Coma cluster ($z = 0.0231$), $D_L$=100.7 Mpc, and 1 arcsec = 0.466 kpc.

## 2 OBSERVATIONS AND DATA REDUCTION

To further study Coma galaxies at radio frequencies, we obtained 1.4 GHz continuum and H I data with the NRAO[1] Karl G. Jansky Very Large Array (VLA) in its B-configuration in two fields centred at NGC 4848 and D100, respectively (Fig. 1), from 2016 June 1st to 11th (Table 1, program code: SH0174, PI: Sun). The 1.4 GHz continuum data were taken with two base bands (A0/C0 and B0/D0) covering a frequency range from 0.9 to 2.1 GHz; each base band is constructed with seven spectral windows of 128 MHz, and each spectral window is divided into 64 channels of 2 MHz. The H I spectral data were taken with two spectral windows (one for A0/C0 and the other for B0/D0) of 64 MHz covering a velocity range of 1000–11 200 km s$^{-1}$. Each spectral window is divided into 3584 channels of 17.8 kHz (or 3.88 km s$^{-1}$ velocity resolution).

The VLA was in the B-configuration for all the observations. 3C 286 was observed to calibrate the flux density scale and the bandpass. J1310+3220 was observed for the calibration of antenna gains and phase. The data were calibrated and reduced with the CASA software; each field was calibrated separately. Beyond the standard CASA pipeline, we removed radio frequency interference (RFI) carefully with the tfcrop and rflag mode of the flagdata task in CASA. About 40 per cent of the data in the continuum band and 20 per cent of the data in the H I band are identified as affected by RFI. Then, phase self-calibration was applied to the continuum data as there are strong sources (15–40 mJy beam$^{-1}$) in the fields that left residuals after the standard calibration. Complex gain calibration solutions were obtained with a 60 s integration time sampling over 1–3 cycles of phase self-calibration until no further significant improvement was obtained. Amplitude self-calibration was tested but was not applied as this brought no further improvements.

To create the H I cube, continuum was carefully fitted with line free channels in the range of ±1000 km s$^{-1}$ centred on the systemic velocity of each RPS galaxy; the continuum was subtracted with the uvcontsub algorithm. Multiscale, multifrequency, multiterm synthesis with w-projection (that is a wide-field imaging technique) were used in the tclean algorithm to clean the continuum and H I data. The continuum map used a robust weighting of 0.5 to get a good compromise between optimized spatial resolution and sensitivity. The H I cube used natural weighting to get the best sensitivity.

## 3 RESULTS AND ANALYSIS

### 3.1 1.4 GHz continuum sources

The overall radio continuum map of the two observed fields is shown in Appendix A. The PYBDSF[2] source-detection package (Mohan & Rafferty 2015) was used to locate and measure the flux densities of the radio sources from our data. PYBDSF calculated the local rms for each pixel, evaluated over a 5 arcmin box. Then, source peaks greater than 4$\sigma$ are identified and all contiguous pixels higher than 2$\sigma$ are identified as belonging to one source. Finally, Gaussian fitting is used to resolve the source position and flux density. In total, 1975 and 1173 radio sources (64 of them are duplicates) are detected within the 10 per cent response of field 1 and 2, respectively. Our source number density is 13.8 (for field 1) and 3.9 (for field 2) times of that from Miller et al. (2009) in the central 6.4 arcmin (90 per cent response radius of the VLA field at 1.4 GHz). To assess the reliability of our flux density measurement, we compared our results with those from Miller et al. (2009) and the FIRST survey (White et al. 1997) (see Appendix B for details). Our flux density is consistent with both.

---

[1] The National Radio Astronomy Observatory is a facility of the National Science Foundation operated under cooperative agreement by Associated Universities, Inc.

[2] http://www.astron.nl/citt/pybdsm/

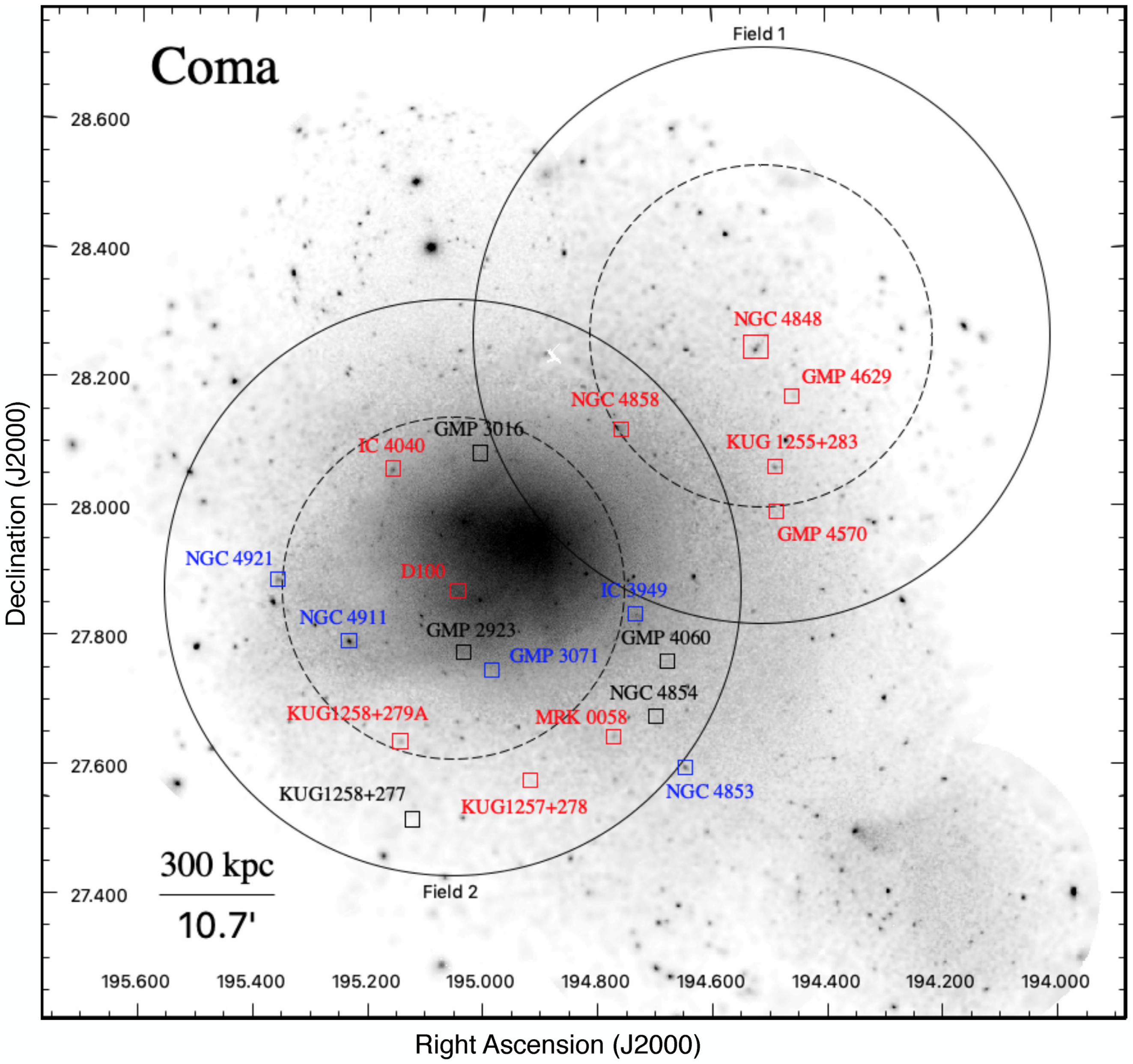

**Figure 1.** *XMM–Newton* 0.4–1.3 keV image of the Coma cluster (Snowden et al. 2008), with positions of the RPS galaxies marked (Smith et al. 2010; Yagi et al. 2010; Kenney, Abramson & Bravo-Alfaro 2015). The RPS galaxies with radio continuum detection in both the galaxy and tail (red), only in the galaxy (blue), and without detection (black) are marked with boxes. The solid and dashed circles show the 10 per cent and 50 per cent response (26.77 arcmin and 15.88 arcmin in radius) of the two VLA fields.

**Table 1.** VLA 1.4 GHz observations in B-configuration.

| Field | RA (J2000) | Dec. (J2000) | Obs. date | Total time (on-source) | Continuum beam | H I beam | Central source |
|---|---|---|---|---|---|---|---|
| 1 | $12^{\mathrm{h}}58^{\mathrm{m}}02\overset{\mathrm{s}}{.}65$ | $+28^{\circ}15'50\overset{''}{.}0$ | 2016 Jun 1–11 | 5 × 3 h (12.1 h) | 4.1 arcsec × 3.5 arcsec | 6.2 arcsec × 5.2 arcsec | NGC 4848 |
| 2 | $13^{\mathrm{h}}00^{\mathrm{m}}12\overset{\mathrm{s}}{.}46$ | $+27^{\circ}52'23\overset{''}{.}4$ | 2016 Jun 5–10 | 2 × 4 h (6.3 h) | 4.7 arcsec × 3.7 arcsec | 7.5 arcsec × 5.2 arcsec | D100 |

With PYBDSF, we also derive the rms distribution for each field. The rms in the centre of fields 1 and 2 are 6 and 8 μJy that are 4 and 3 times deeper than the Miller et al. (2009) data. Because of the primary beam correction, the rms increases from the centre of the field to the outer regions. As NGC 4848 and D100 are at the centre of their fields, they have the deepest data in their

**Table 2.** Coma RPS galaxies studied in this paper.

| NO. | galaxy | RA (J2000) $(^{\rm h\ m\ s})$ | Dec. (J2000) $(^{\circ\ \prime\ \prime\prime})$ | Velocity (km s$^{-1}$) | Rms ($\mu$Jy beam$^{-1}$) | 1.4 GHz flux density (mJy) | Field |
|---|---|---|---|---|---|---|---|
| 1 | NGC 4848 (GMP 4471) | 12 58 05.59 | 28 14 33.6 | 7184 | 5.94 | 23.85 ± 0.11 | 1 |
| 2 | KUG 1255+283 (GMP 4555) | 12 57 57.74 | 28 03 42.1 | 8136 | 8.04 | 6.76 ± 0.08 | 1 |
| 3 | NGC 4858 (GMP 3816) | 12 59 02.11 | 28 06 56.4 | 9416 | 9.85 | 8.73 ± 0.13 | 1 |
| 4 | GMP 4570 | 12 57 56.81 | 27 59 30.6 | 4565 | 9.92 | 0.55 ± 0.06 | 1 |
| 5 | GMP 4629 | 12 57 50.27 | 28 10 13.7 | 6918 | 5.73 | 0.03 ± 0.01 | 1 |
| 6 | D100 (MRK 0060, GMP 2910) | 13 00 09.15 | 27 51 59.4 | 5316 | 8.05 | 1.12 ± 0.03 | 2 |
| 7 | KUG 1258+279A (GMP 2599) | 13 00 33.70 | 27 38 15.6 | 7485 | 13.8 | 3.70 ± 0.09 | 2 |
| 8 | MRK 0058 (GMP 3779) | 12 59 05.30 | 27 38 39.6 | 5419 | 19.5 | 3.29 ± 0.15 | 2 |
| 9 | IC 4040 (GMP 2559) | 13 00 37.91 | 28 03 28.0 | 7675 | 10.7 | 16.31 ± 0.10 | 2 |
| 10 | KUG 1257+278 (GMP 3271) | 12 59 39.82 | 27 34 35.9 | 5011 | 17.7 | 0.51 ± 0.07 | 2 |
| 11 | IC 3949* (GMP 3896) | 12 58 55.89 | 27 49 59.9 | 7526 | 14.5 | 2.37 ± 0.09 | 2 |
| 12 | GMP 3071* | 12 59 56.15 | 27 44 47.3 | 8920 | 9.04 | 0.05 ± 0.02 | 2 |
| 13 | NGC 4853* (GMP 4156) | 12 58 35.20 | 27 35 47.1 | 7688 | 40.8 | 1.35 ± 0.15 | 2 |
| 14 | NGC 4911* (GMP 2374) | 13 00 56.08 | 27 47 26.9 | 7985 | 10.4 | 15.08 ± 0.23 | 2 |
| 15 | NGC 4921* (GMP 2059) | 13 01 26.15 | 27 53 09.5 | 5470 | 14.6 | 0.44 ± 0.05 | 2 |
| 16 | GMP 4060* | 12 58 42.60 | 27 45 38.0 | 8686 | 20.8 | <0.083 | 2 |
| 17 | NGC 4854* (GMP 4017) | 12 58 47.44 | 27 40 29.3 | 8383 | 24.6 | < 0.098 | 2 |
| 18 | GMP3016* | 13 00 01.08 | 28 04 56.2 | 7765 | 10.8 | < 0.043 | 2 |
| 19 | GMP 2923* | 13 00 08.07 | 27 46 24.0 | 8672 | 8.54 | < 0.034 | 2 |
| 20 | KUG 1258+277* (GMP 2640) | 13 00 29.23 | 27 30 53.7 | 7395 | 23.6 | < 0.094 | 2 |

*Note.* The properties of 20 RPS galaxies from Smith et al. (2010), Yagi et al. (2010), and Kenney et al. (2015) are listed. RA, Dec., and optical velocity are from LEDA (Makarov et al. 2014), except for GMP3016 whose velocity is from NED as there is no LEDA value. The local rms and continuum flux density (or 4$\sigma$ upper limit) measured by PYBDSF are also shown for each galaxy. The rms varies within the same field because of the primary beam correction. The synthesized beam sizes are shown in Table 1. galaxies with an asterisk have no RPS tails detected in radio continuum.

respective fields. The full continuum source catalogue is shown in Table B1.

### 3.2 Radio continuum emission of RPS galaxies

20 RPS galaxies (Smith et al. 2010; Yagi et al. 2010; Kenney et al. 2015) are covered by our observations. Their radio properties, measured from our data, are listed in Table 2. 15 of them are detected in the radio continuum, while the other five (GMP 4060, NGC 4854, GMP 3016, GMP 2923, and KUG 1258+277) were not detected (Table 2).

We detected significant extended radio emission coincident with the H$\alpha$ or SF tails in 10 of the 20 RPS galaxies (Fig. 2 and Table 3), or in 10 of 15 (66 per cent) RPS galaxies detected at 1.4 GHz, unambiguously revealing the widespread occurrence of relativistic electrons and magnetic fields in the stripped tails. Radio tails behind IC 4040 and KUG 1255+283 were reported in Miller et al. (2009), while the other 8 are new. The galaxy regions and tail regions are visually defined based on the radio continuum maps (Fig. 2). Symmetrical discs are defined as galaxy regions from radio continuum map by means of circles/ellipses/rectangles. The one-sided asymmetric structures extending beyond the galaxy regions are defined as tails (solid rectangles). Both galaxy regions and tail regions were set to match approximately the 2$\sigma$ contour of the radio emission. The 1.4 GHz continuum flux densities of galaxies and tails are listed in Table 3.

The radio continuum tail is always spatially coincident with the H$\alpha$ or SF tail but usually shorter than either (except for KUG 1257+278), at least at the sensitivity level of the current radio data. All tails, except for KUG 1257+278, extend beyond $D_{25}$ (diameter of a galaxy at an isophotal level of 25 mag arcsec$^{-2}$ in the $B$ band, taken from LEDA, Makarov et al. 2014).

The in-band spectral index was also derived, taking advantage of the wide bandwidth covered by the correlator. Because of the weak signal in general, we divided the 1.4 GHz continuum into two parts, a low frequency (approximately 0.9–1.5 GHz) and a high frequency one (approximately 1.5–2.1 GHz). Then flux density maps centred at 1.25 and 1.75 GHz were created, and the power-law index for the galaxy and tail was derived using the convention of $S \sim \nu^{\alpha}$. We only measure the spectral index of a region when it is detected above 5$\sigma$ in both bands. The results are shown in Table 3 and Fig. 3. Our results hint that the tail has a steeper spectrum than the galaxy, which is consistent with aging of electrons and a lack of fresh injection of relativistic electrons in the tails. But the limited depth and frequency coverage of our data do not allow us to reach a definite conclusion.

### 3.3 H I emission of RPS galaxies

The H I data have a spatial resolution of ~6 arcsec using natural weighting to match the narrow width of the gaseous stripped tails of RPS galaxies. The sensitivities of the H I spectra for 20 RPS galaxies are listed in Table 4. Although our high spatial resolution H I data are less sensitive than the low-resolution data from Bravo-Alfaro et al. (2000) (observed in C-configuration with the VLA) for sources with radii larger than 30 arcsec, the better spatial resolution can resolve the peak H I structure of galaxies and give better H I upper limits for small galaxies and narrow tails, such as D100's tail that is discussed in Section 4.2.2.

H I emission is detected in the integrated intensity (moment 0) maps for NGC 4848, NGC 4911, and IC 4040 as shown in Fig. 4. The H I integrated intensity maps are made from the H I cubes with 2$\sigma$ 3D masks created by SOFIA (Serra et al. 2015). The $D_{25}$ regions are also indicated in Fig. 4. The gap in the $D_{25}$ region for NGC 4848 is the result of a mask which was applied to remove an image side-lobe artefact. The positions of H I emission peaks in the integrated

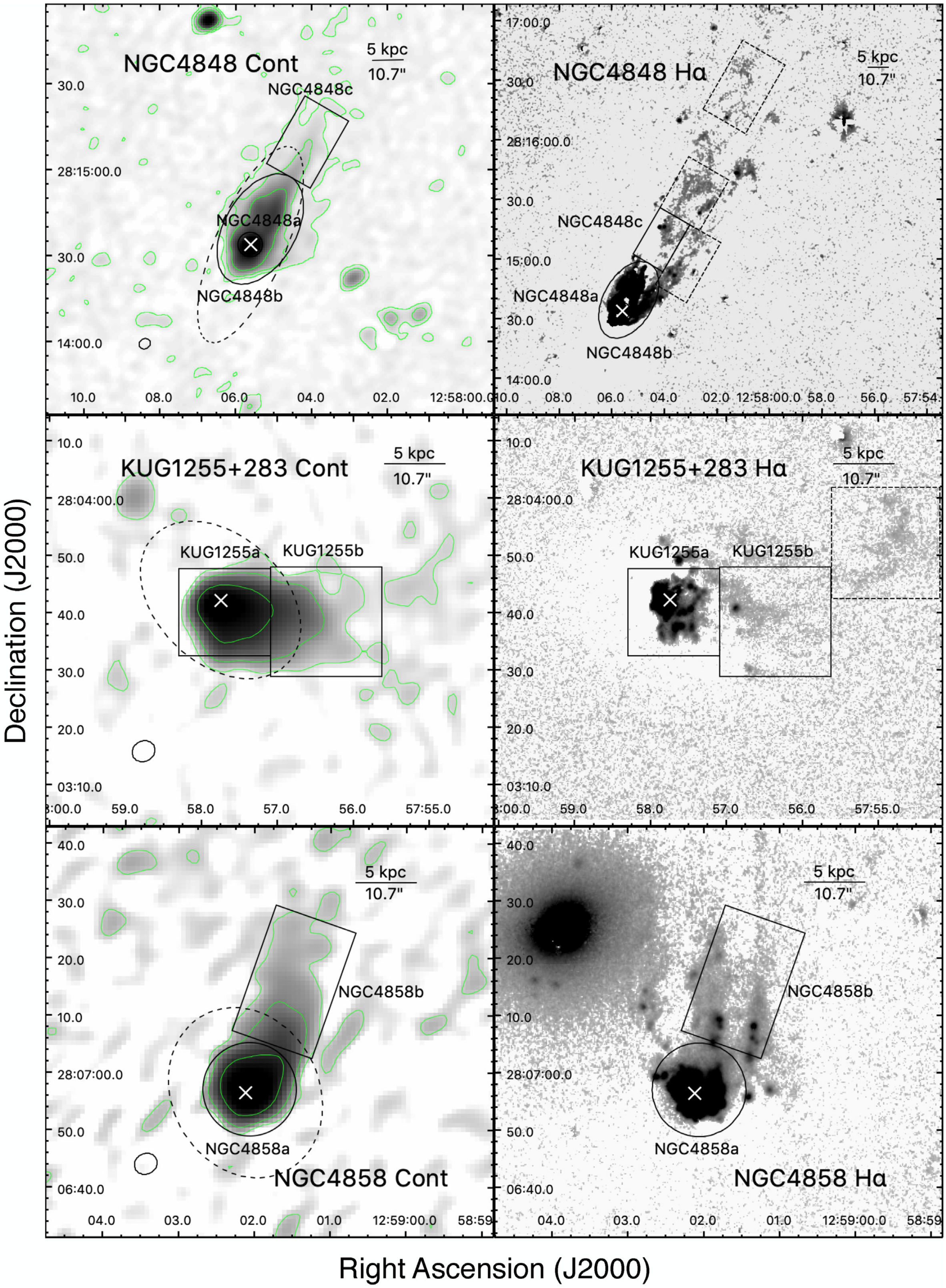

**Figure 2a.** Left: VLA 1.4 GHz continuum images for RPS galaxies. Green contours show $2\sigma$, $10\sigma$, and $50\sigma$ flux density levels in the radio continuum. Radio emission in galactic discs is measured in symmetrical regions around galaxy centres outlined by solid circles, or ellipses, or rectangles. Radio emission in one-sided asymmetric tails is also measured in regions shown by solid rectangles. Dashed black ellipses show $D_{25}$. Right: H $\alpha$ maps for the same galaxies from the *Subaru* data, except for KUG 1258+279A and NGC 4921 (H $\alpha$ map from GOLDMine, Gavazzi et al. 2003). The nuclei are marked with a white X. The dashed boxes are where H $\alpha$ emission and upper limits on the radio continuum emission are measured, the values of which are included in Fig. 6. The dashed line in the KUG 1258+279A H $\alpha$ map points along the direction that Smith et al. (2010) identified as the ‘tail’.

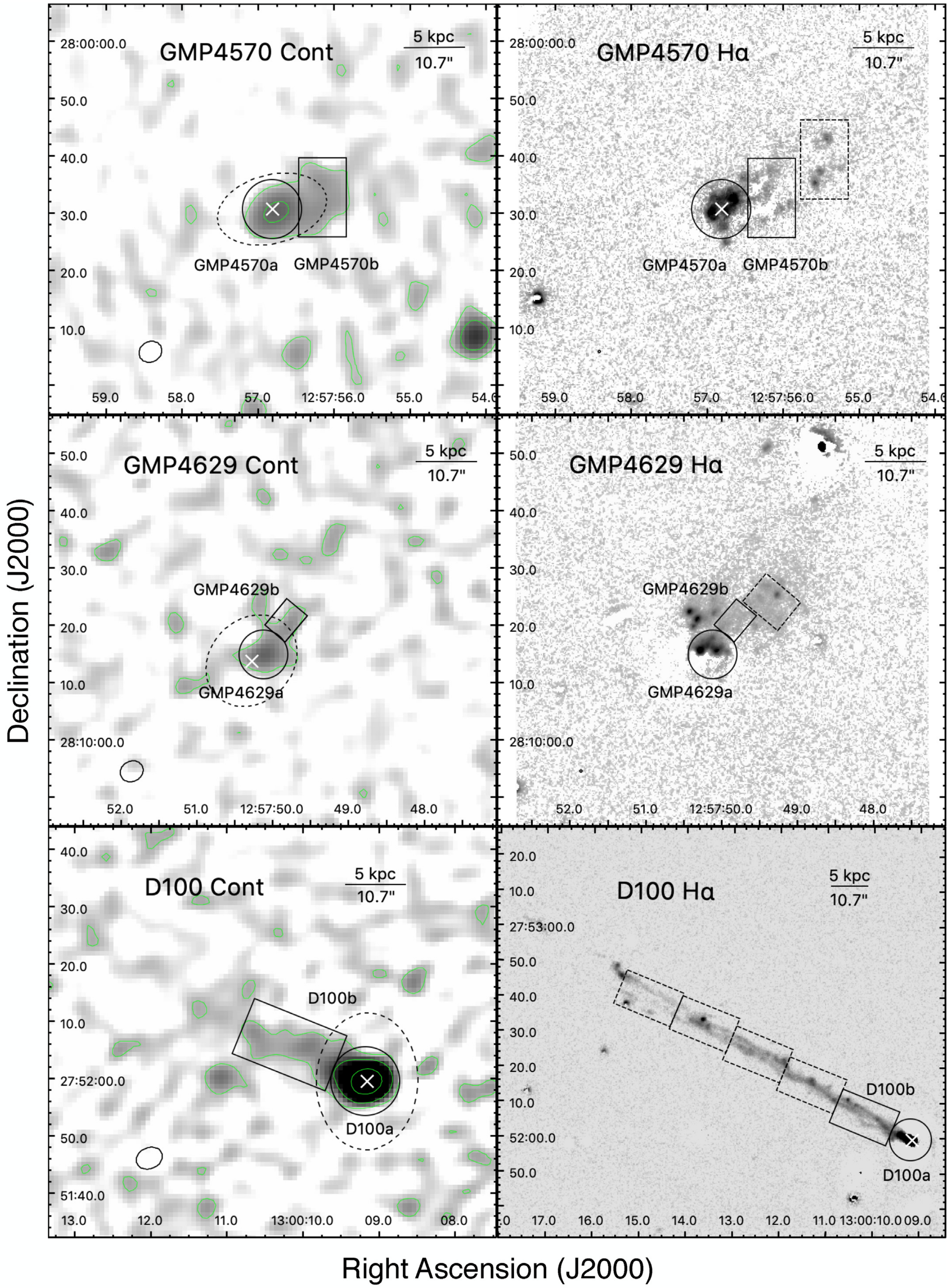

**Figure 2b.** *Continued.*

intensity maps are consistent with those from Bravo-Alfaro et al. (2000). Corresponding H I spectra for the $D_{25}$ regions are shown in Fig. 5 and the H I results are listed in Table 5. The H I flux within the SOFIA 3D mask (H I Flux$_{\mathrm{SoFiA}}$) is lower than that within $D_{25}$ (H I Flux$_{\mathrm{D25}}$), revealing that there is some weak H I emission within $D_{25}$ that was not picked up by SOFIA, especially for NGC 4911. Increasing the radii of the areas of integration to twice $D_{25}$ does not lead to a further increase in H I flux, suggesting that we have measured the

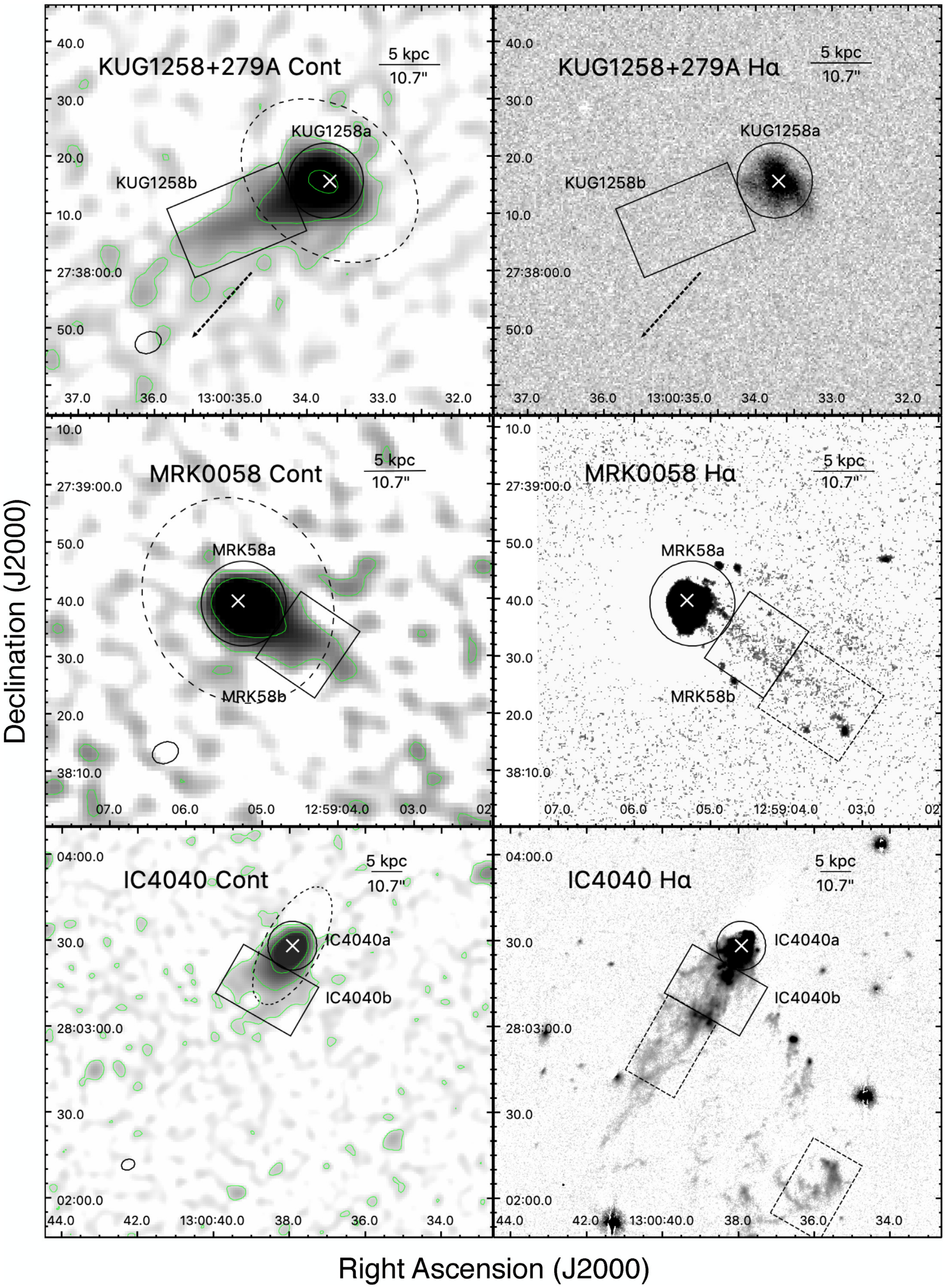

**Figure 2c.** *Continued.*

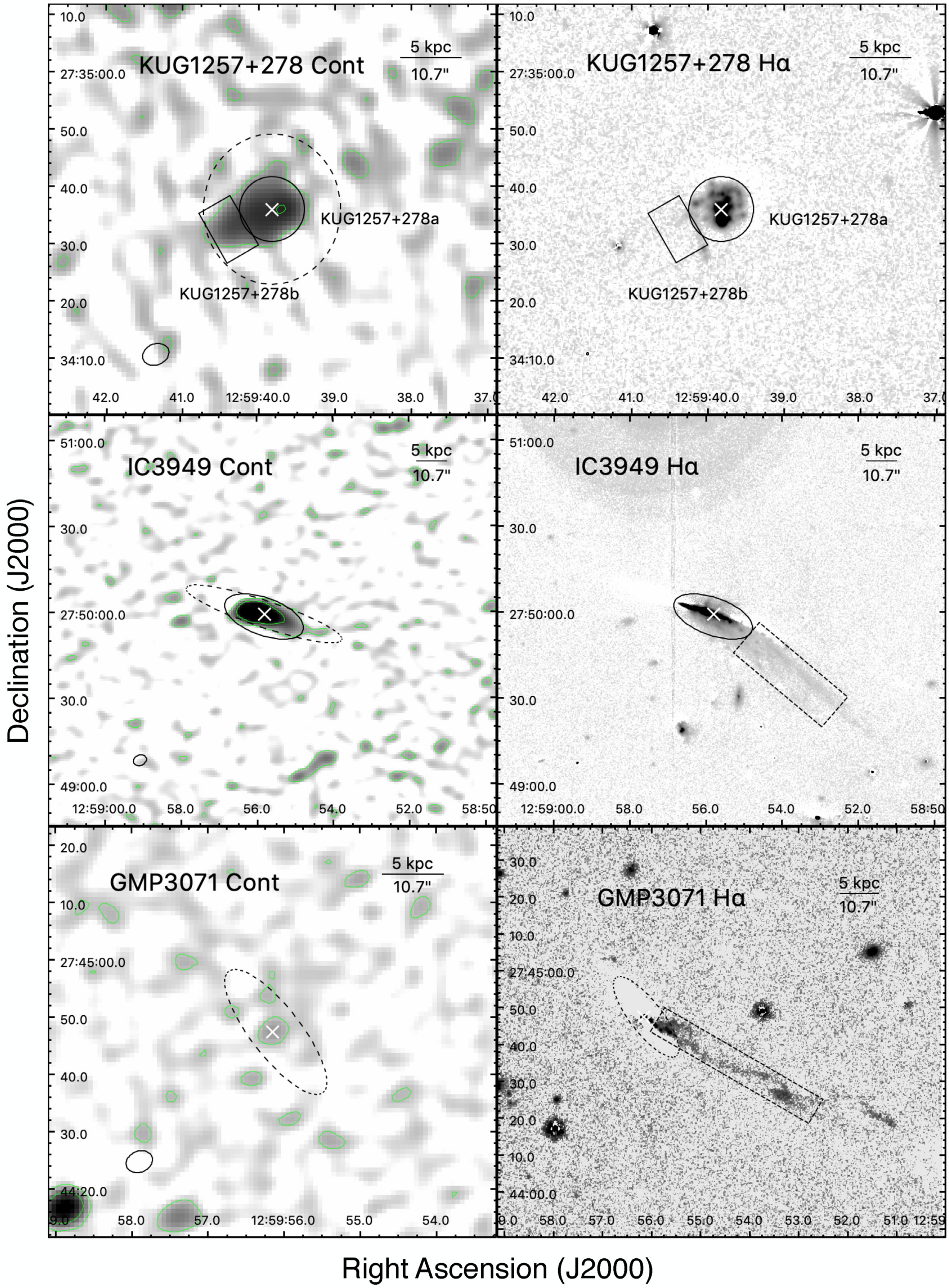

**Figure 2d.** *Continued.*

total flux within $D_{25}$. Our H I Flux$_{D25}$ is larger than H I Flux$_{BA00}$; these may be because Bravo-Alfaro et al. (2000) ignored the diffuse H I emission within $D_{25}$ where the S/N ratio is lower than 3.

Six galaxies (NGC 4848, MRK 0058, KUG 1258+279A, IC 4040, NGC 4911, and NGC 4921) in our sample are detected in H I by Bravo-Alfaro et al. (2000), three of which (MRK 0058, KUG

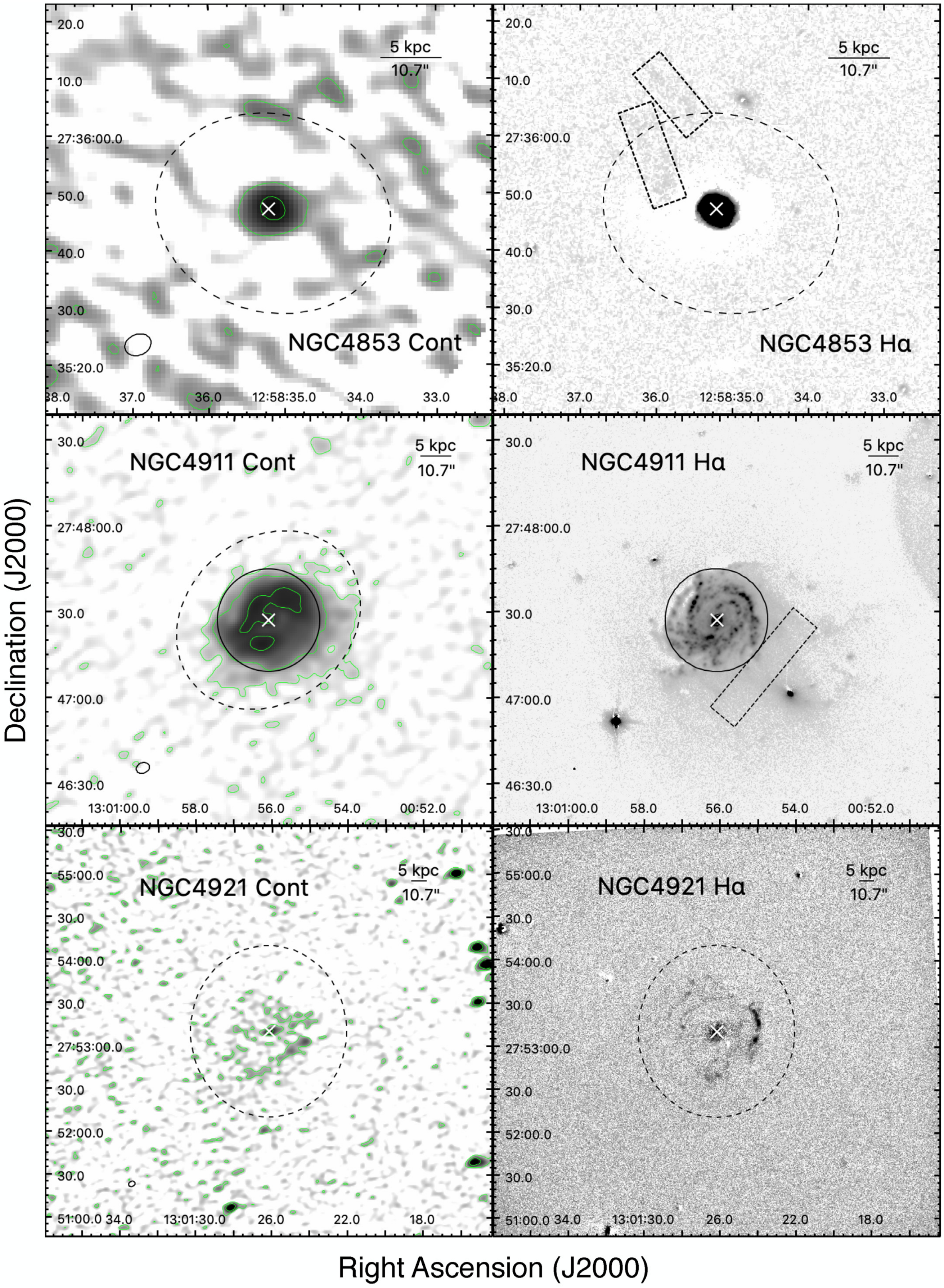

**Figure 2e.** *Continued.*

**Table 3.** Radio continuum flux densities of RPS galaxies and their tails.

| NO. | Region identification | Component | 1.4 GHz flux density (mJy) | Spectral index | Sky area (arcsec$^2$) | Tail length (kpc) |
|---|---|---|---|---|---|---|
| 1 | NGC 4848a | Nucleus | 9.495 ± 0.011 | – 0.55 ± 0.01 | 58.2 | – |
| 1 | NGC 4848b | galaxy | 13.207 ± 0.041 | – 0.82 ± 0.02 | 769.3 | – |
| 1 | NGC 4848c | Tail | 0.851 ± 0.032 | – 0.97 ± 0.33 | 472.3 | 12.6 |
| 2 | KUG1255+283a | galaxy | 5.476 ± 0.032 | – 1.03 ± 0.05 | 256.0 | – |
| 2 | KUG1255+283b | Tail | 1.366 ± 0.038 | – 1.36 ± 0.25 | 368.6 | 9.1 |
| 3 | NGC4858a | galaxy | 6.865 ± 0.035 | – 1.32 ± 0.05 | 209.3 | – |
| 3 | NGC4858b | Tail | 1.245 ± 0.045 | – 2.25 ± 0.49 | 341.8 | 10.8 |
| 4 | GMP 4570a | galaxy | 0.297 ± 0.023 | – 1.08 ± 0.82 | 84.5 | – |
| 4 | GMP 4570b | Tail | 0.207 ± 0.026 | – | 108.8 | 3.9 |
| 5 | GMP 4629a | galaxy | 0.066 ± 0.011 | – | 59.5 | – |
| 5 | GMP 4629b | Tail | 0.023 ± 0.007 | – | 26.9 | 2.8 |
| 6 | D100a | galaxy | 1.099 ± 0.019 | – 0.64 ± 0.15 | 113.9 | – |
| 6 | D100b | Tail | 0.154 ± 0.024 | – | 179.2 | 8.1 |
| 7 | KUG1258+279Aa | galaxy | 2.845 ± 0.033 | – 1.25 ± 0.12 | 134.4 | – |
| 7 | KUG1258+279Ab | Tail | 1.070 ± 0.048 | – 1.58 ± 0.51 | 273.3 | 9.8 |
| 8 | MRK58a | galaxy | 2.585 ± 0.058 | – 2.13 ± 0.31 | 173.4 | – |
| 8 | MRK58b | Tail | 0.486 ± 0.058 | – | 173.4 | 5.8 |
| 9 | IC 4040a | galaxy | 14.105 ± 0.036 | – 1.22 ± 0.02 | 228.5 | – |
| 9 | IC 4040b | Tail | 2.507 ± 0.059 | – 1.41 ± 0.23 | 589.4 | 9.1 |
| 10 | KUG1257+278a | galaxy | 0.584 ± 0.040 | – | 101.1 | – |
| 10 | KUG1257+278b | Tail | 0.200 ± 0.031 | – | 61.4 | 2.9 |

*Note.* The properties of radio continuum for each galaxy/tail region defined in the radio continuum maps of Fig. 2 are listed. Sky area refers to the solid angle for each galaxy/tail region. The length of tails is estimated with a cut off at $2\sigma$.

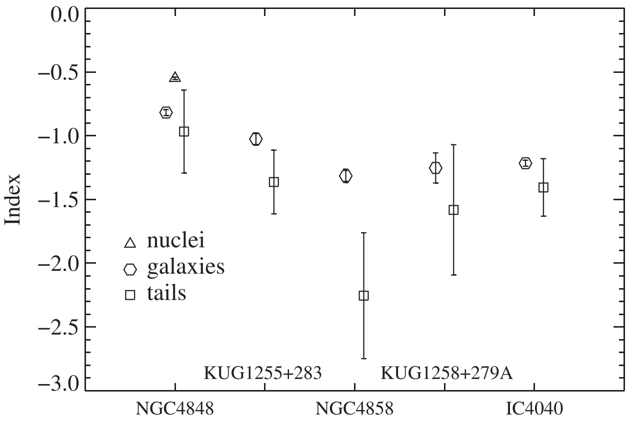

**Figure 3.** The in-band spectral index for the nucleus, galaxy, and tail regions of five RPS galaxies with the spectral index in the tail constrained.

1258+279A, and NGC 4921) are not detected in this work. The H I in these three galaxies is probably of an extended nature and lacks bright clumps. Also, these galaxies fall at about the 50 per cent response radius of field 2 so the sensitivity of the data may not be good enough.

## 4 DISCUSSION

### 4.1 The nature of the radio continuum emission of the stripped tails

The observed 1.4 GHz continuum should be dominated by synchrotron radiation. Typically for spiral galaxies, the radio continuum emission is a tracer for SF as relativistic electrons are accelerated by core-collapse supernovae (e.g. Condon, Anderson & Helou 1991; Bell 2003; Murphy et al. 2008). As H II regions (tracing massive stars) have been found in stripped tails (Gavazzi et al. 1995; Sun et al. 2007; Cramer et al. 2019), the local supernovae could contribute to the synchrotron radiation in tails. On the other hand, relativistic electrons can be stripped by ram pressure as in radio head–tail galaxies (e.g. Gavazzi & Jaffe 1987; Murphy et al. 2009). In the following, we investigate if the observed radio continuum emission is mainly related to SF in the tail or due to relativistic electrons that were stripped from the galaxy by ram pressure.

#### *4.1.1 Radio continuum versus H α and IR*

We compared the 1.4 GHz continuum and H $\alpha$ surface brightness (SB) in tails (blue) and galaxies (red) in Fig. 6, to study the origin of the radio tails. Each number indicates a galaxy as listed in Table 2. Blue arrows show $3\sigma$ 1.4 GHz SB upper limits for the dashed box regions in Fig. 2. The 1.4 GHz SB is the ratio between 1.4 GHz flux density and sky area (listed in Table 3) for each tail/galaxy region defined in Fig. 2. H $\alpha$ SB values for the same tail/galaxy regions are estimated from the *Subaru* data as in Yagi et al. (2017), except that of KUG 1258+279A which is from GOLDMine. Broad-band oversubtraction and [N II], [S II], and [O I] contamination are corrected. The intrinsic extinction is unknown. About 1 mag of intrinsic extinction was measured for two isolated H II regions in the Virgo cluster (Gerhard et al. 2002; Cortese et al. 2004). We simply adopt this value on our H $\alpha$ SB.

If the relativistic electrons emitting radio in stripped tails come from local supernovae in the tails, it is expected that the same 1.4 GHz–H $\alpha$ relation in galaxies will be followed. However, all

**Table 4.** H I deficiency for late-type galaxies in the Coma cluster.

| NO. | galaxy | Type | $D_{25}$ (arcsec) | $M_{\rm H\,I\,normal}$ ($10^8$ M$_\odot$) | Rms$_{\rm H\,I}$ (μJy beam$^{-1}$) | $m_{\rm B}$ (mag) | $i$ (deg) | $M_{\rm H\,I}$ ($10^8$ M$_\odot$) | Def$_{\rm H\,I}$ | Def$_{\rm HI\_BA00}$ |
|---|---|---|---|---|---|---|---|---|---|---|
| 1 | NGC 4848 (GMP 4471) | Scd | 73.8 | 87.7 | 149 | 13.43 | 73.9 | 19.99 | 0.64 | 1.14 |
| 2 | KUG 1255+283 (GMP 4555) | I | 32.2 | 16.7 | 284 | 15.55 | 47.4 | <5.58 | >0.48 | – |
| 3 | NGC 4858 (GMP 3816) | Sbc | 30.8 | 14.6 | 362 | 15.42 | 35.6 | <6.77 | >0.33 | >0.93 |
| 4 | GMP 4570 | I | 19.4 | 6.1 | 395 | 16.74 | 59.5 | <4.05 | >0.18 | – |
| 5 | GMP 4629 | N/A | 17.3 | 4.2 | 207 | 17.13 | 37.8 | <1.77 | >0.38 | – |
| 6 | D100 (MRK 0060, GMP 2910) | I | 23.9 | 9.2 | 246 | 15.83 | 45.0 | <3.20 | >0.46 | – |
| 7 | KUG 1258+279A (GMP 2599) | Sb | 33.7 | 16.7 | 440 | 15.32 | 44.6 | <8.64 | >0.29 | 0.58 |
| 8 | MRK 0058 (GMP 3779) | Sb | 37.0 | 20.1 | 788 | 14.98 | 31.1 | <16.61 | >0.08 | 0.51 |
| 9 | IC 4040 (GMP 2559) | Scd | 45.5 | 33.3 | 388 | 14.60 | 83.6 | 7.5 | 0.65 | 0.61 |
| 10 | KUG 1257+278 (GMP 3271) | I | 26.2 | 11.0 | 697 | 16.34 | 24.0 | <7.90 | >0.15 | – |
| 11 | IC 3949 (GMP 3896) | S | 57.3 | 46.0 | 533 | 14.91 | 90.0 | <10.46 | >0.64 | – |
| 12 | GMP 3071 | S0/a | 26.8 | 6.4 | 290 | 16.94 | 90.0 | <2.84 | >0.35 | – |
| 13 | NGC 4853 (GMP 4156) | S0p | 41.5 | 15.2 | 1649 | 14.21 | 40.3 | <47.27 | > − 0.49 | – |
| 14 | NGC 4911 (GMP 2374) | Sb | 68.9 | 69.7 | 326 | 13.44 | 34.7 | 37.34 | 0.27 | 0.58 |
| 15 | NGC 4921 (GMP 2059) | Sb | 119.7 | 210.4 | 504 | 13.34 | 24.8 | <39.85 | >0.72 | 1.11 |
| 16 | GMP 4060 | Sd | 18.1 | 5.3 | 849 | 17.36 | 34.4 | <6.55 | > − 0.09 | – |
| 17 | NGC 4854 (GMP 4017) | S0 | 57.3 | 29.0 | 1019 | 14.77 | 53.8 | <38.35 | > − 0.12 | – |
| 18 | GMP 3016 | N/A | N/A | – | 372 | N/A | N/A | – | – | – |
| 19 | GMP 2923 | E | 18.5 | 3.0 | 267 | 17.32 | 90.0 | <2.13 | >0.15 | – |
| 20 | KUG 1258+277 (GMP 2640) | S0p | 29.4 | 7.6 | 965 | 15.62 | 73.4 | <13.19 | > − 0.24 | >0.7 |

*Note.* The expected H I mass ($M_{\rm H\,I\,normal}$) is derived from table IV of Haynes & Giovanelli (1984) with $D_{25}$ from LEDA and galaxy type from Dressler (1980) (except for GMP 4060 and GMP 2923 from LEDA). For the galaxies without morphology type information (N/A), $M_{\rm H\,I\,normal}$ is derived from the average relation of $M_{\rm H\,I}$ and $D_{25}$ for all the galaxies. The rms$_{\rm H\,I}$ values are calculated for the H I cubes for a channel width of 21.5 km s$^{-1}$. The beam sizes of the H I cubes are shown in Table 1. The values for $m_{\rm B}$ and inclination ($i$) are also from LEDA. N/A means not available. Def$_{\rm HI\_BA00}$ is based on Def$_{\rm H\,I}$ from Bravo-Alfaro et al. (2000).

the RPS galaxies, except IC 4040 (nine in Fig. 6), show a higher 1.4 GHz to H α ratio in the tails than in the galaxies. The mean ratio in the tails ($1.84 \times 10^{14}$ mJy erg$^{-1}$ s cm$^2$, blue dashed line) is 6.8 times that in galaxies ($2.69 \times 10^{13}$ mJy erg$^{-1}$ s cm$^2$, red dashed line). Moreover, H α emission in tails only provides an upper limit on the SFR as the stripping and heating (caused by the RPS shock) of ionized gas can account for much of the diffuse H α emission (e.g. Sun et al. 2010; Fossati et al. 2016; Cramer et al. 2019). So the radio continuum in the Coma tails is generally too strong compared to the value expected from the SFR. Our results suggest that the radio-emitting plasma in tails is not formed *in situ*, but stripped from the galaxy by ram pressure. While the above analysis is based on rectangular regions roughly matching the radio emission, we also examined the change on the results by using tail regions coinciding with a constant SB limit of 20 μJy beam$^{-1}$ (beam size 4.7 arcsec × 3.7 arcsec). Both radio surface brightness and the H α SB have been re-measured with this new set of regions. The averaged 1.4 GHz to H α ratio in the new set of the tail regions is now 46 per cent higher than the blue dashed line in Fig. 6, and the scatter still remains about the same. For simplicity and the sizable scatter here, we stick to the results from the simple rectangular regions as shown in Fig. 2.

There is also evidence that the ram pressure may also enhance the radio emission of the main bodies of the galaxies. With the 70, 100, and 160 μm flux densities for these RPS galaxies from the *Herschel* point source catalogue, the radio–infrared (IR) relations of these RPS galaxies are compared with those for star-forming galaxies (Fig. 7). Because the main bodies are much brighter than the tails, the radio and IR emissions of the RPS galaxies are dominated by their main bodies. The total-IR (TIR, 3–1100 μm) luminosity of the RPS galaxies in the Coma cluster is derived from the 70, 100, and 160 μm flux densities with the calibration coefficients listed in table 3 of Galametz et al. (2013). The corresponding far-IR (FIR, 42–122 μm) fraction was given by the 70–160 μm flux density ratio with the equation 3 of Murphy et al. (2008). The IR to 1.4 GHz ratio is generally expressed by the parameter $q$ (Helou, Soifer & Rowan-Robinson 1985; Bell 2003):

$$q_{\rm IR} = \log_{10}\left(\frac{\rm IR}{3.75 \times 10^{12}\ {\rm W\ m^{-2}}}\right) - \log_{10}\left(\frac{S_{1.4\ \rm GHz}}{\rm W\ m^{-2}\ Hz^{-1}}\right). \quad (1)$$

The mean values of $q_{\rm TIR}$ and $q_{\rm FIR}$ in the RPS galaxies of the Coma cluster ($q_{\rm TIR} = 2.38 \pm 0.25$ and $q_{\rm FIR} = 2.05 \pm 0.24$, the red dashed lines in Fig. 7) are systematically lower than that in star-forming galaxies ($q_{\rm TIR} = 2.64 \pm 0.26$ and $q_{\rm FIR} = 2.34 \pm 0.26$, the black solid lines in Fig. 7, Bell 2003; Yun et al. 2001). On average, the 1.4 GHz continuum in the RPS galaxies in the Coma cluster is enhanced relative to their TIR (by a factor of 1.9) and FIR (by a factor of 2.0) compared to normal star-forming galaxies. Previous works also reported the radio excess in the Coma cluster galaxies (e.g. Gavazzi & Jaffe 1986; Gavazzi, Boselli & Kennicutt 1991) and in the Virgo cluster galaxies (e.g. Murphy et al. 2009; Vollmer et al. 2013). The mean $q_{\rm TIR}$ and $q_{\rm FIR}$ in the Virgo cluster galaxies are $2.50 \pm 0.12$ and $2.04 \pm 0.20$ (the blue dashed lines in Fig. 7, Murphy et al. 2009). Several mechanisms have been proposed to explain the enhanced radio continuum in RPS galaxies, including the enhancement of magnetic field strength caused by ISM shear motions (Murphy et al.

2009), the compression of ISM/magnetic field by the ICM ram and/or thermal pressure (Murphy et al. 2009), and turbulence and ICM shocks caused by ram pressure (Kang & Ryu 2011). The general radio enhancement in the Coma tails may be related to turbulence in the tail and wake of the galaxy, a further investigation of which would require more theoretical or simulation work which is beyond the scope of this paper.

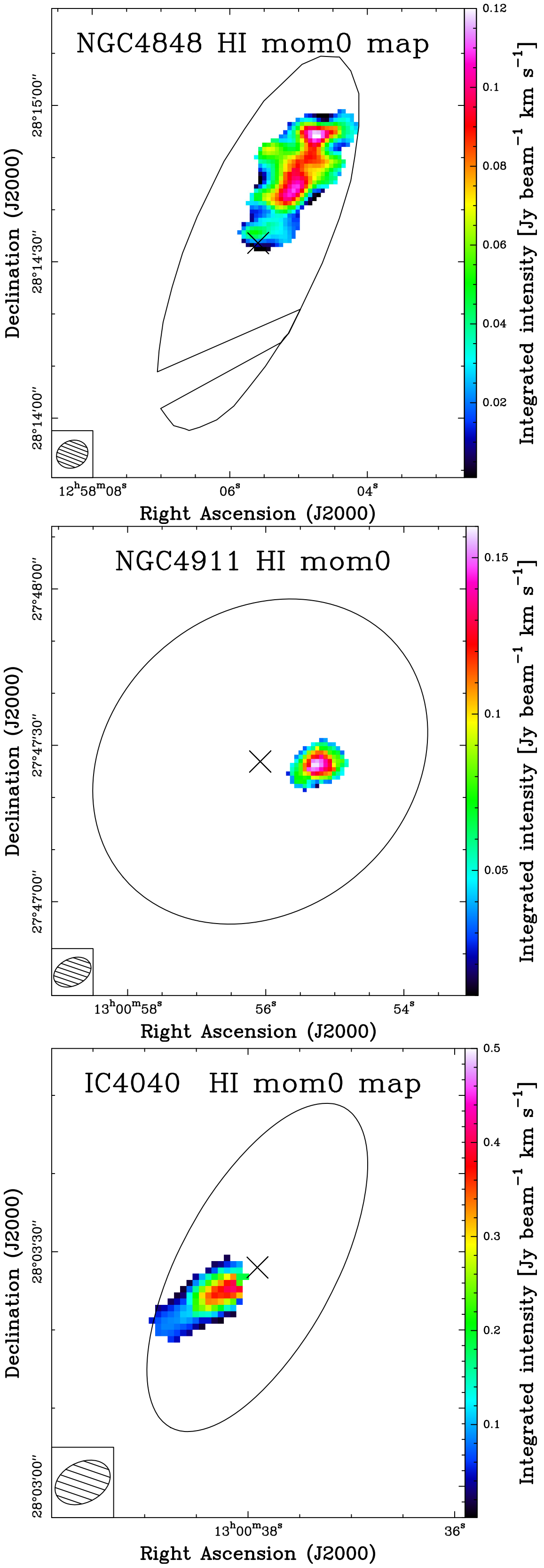

**Figure 4.** Integrated intensity (moment 0) map of H I within the 2$\sigma$ 3D mask created by SOFIA. The beam size is listed in Table 1. Black ellipses show the $D_{25}$ regions. The nuclei of galaxies are shown as black X.

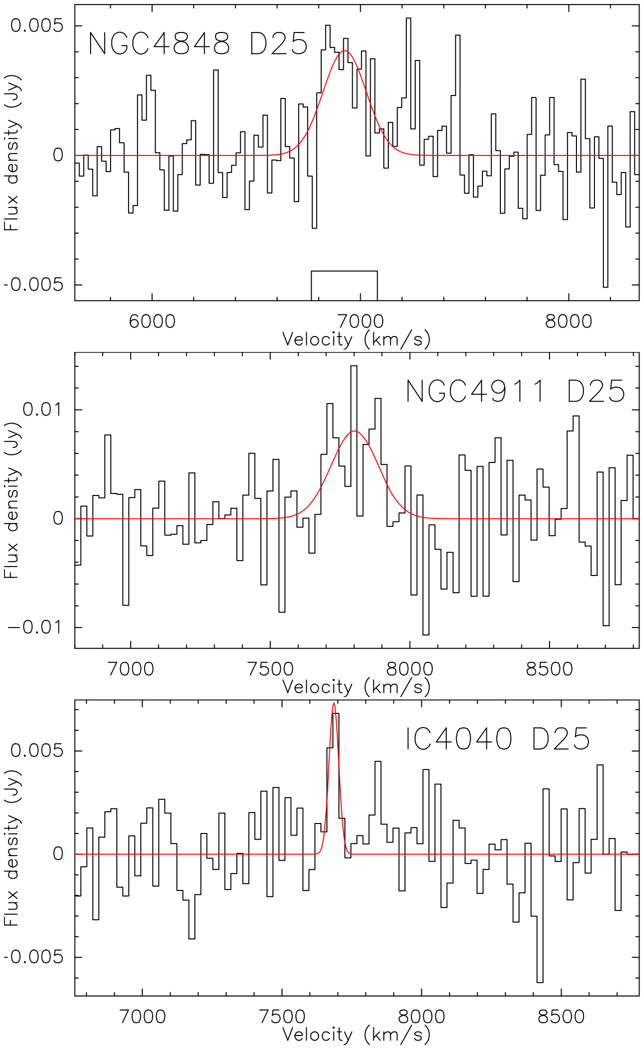

**Figure 5.** H I spectra for the $D_{25}$ regions of three galaxies with H I detected. The H I spectra are fitted with a Gaussian function shown as the red line.

**Table 5.** H I flux of RPS galaxies.

| galaxy | H I Flux$_{\mathrm{SOFIA}}$ (Jy km s$^{-1}$) | H I Flux$_{\mathrm{D25}}$ (Jy km s$^{-1}$) | H I Flux$_{\mathrm{BA00}}$ (Jy km s$^{-1}$) |
|---|---|---|---|
| NGC 4848 | $0.464 \pm 0.005$ | $0.878 \pm 0.132$ | $0.37 \pm 0.03$ |
| NGC 4911 | $0.136 \pm 0.004$ | $1.64 \pm 0.32$ | $0.80 \pm 0.07$ |
| IC 4040 | $0.260 \pm 0.005$ | $0.33 \pm 0.11$ | $0.29 \pm 0.06$ |

*Note.* H I Flux$_{\mathrm{SOFIA}}$ is the H I flux calculated in the 2$\sigma$ 3D mask created by SOFIA. H I Flux$_{\mathrm{D25}}$ is calculated in the $D_{25}$ region defined in the optical (black ellipse in Fig. 4). H I Flux$_{\mathrm{BA00}}$ is measured by Bravo-Alfaro et al. (2000).

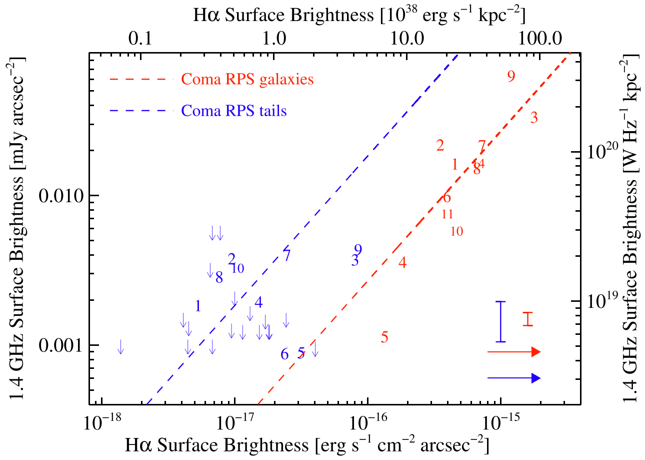

**Figure 6.** The 1.4 GHz SB versus H $\alpha$ surface brightness for RPS galaxies and their tails in regions defined in Fig. 2. Each number indicates a galaxy as listed in Table 2, and tails are in blue and galaxies are in red. Blue arrows are 1.4 GHz upper limits for the dashed box regions in Fig. 2 where an H $\alpha$ tail is detected but a radio extension is absent from the current data. Bottom right arrows show the extinction correction of one magnitude applied on H $\alpha$. The mean ratios of 1.4 GHz to H $\alpha$ for RPS tails and galaxies in the Coma cluster are shown as blue and red dashed lines, respectively.

### 4.1.2 *Synchrotron cooling time*

If the 1.4 GHz emission in the stripped tail originates from the relativistic electrons stripped from the galaxy by ram pressure, the relativistic electrons will cool/age along the tail. The age of the relativistic electrons in the tail, $t$, is roughly $d/v$, where $d$ is the distance from the galaxy and $v$ is the mean velocity of electrons stripped from the galaxy. The 1.4 GHz emission can only be detected before the relativistic electrons have cooled, or roughly $t < t_{\rm syn}(1.4\ {\rm GHz})$, which is equivalent to $d < t_{\rm syn}(1.4\,{\rm GHz}) \times v$, where $t_{\rm syn}(1.4\ {\rm GHz})$ is the synchrotron cooling time at 1.4 GHz. With this assumption, if the tail length detected at 1.4 GHz does not exceed $t_{\rm syn}(1.4\,{\rm GHz}) \times v$, it will support the assumption that the bulk of the radio continuum in tails is stripped from the galaxy.

Using equation 9 of Feretti & Giovannini (2008), the synchrotron cooling time (in Myr) can be estimated as

$$t_{\rm syn}(\nu) = 1590 \frac{B^{0.5}}{B^2 + B_{\rm CMB}^2}[(1+z)\nu]^{-0.5}, \qquad (2)$$

where the magnetic field $B$ is in μG, the frequency is in GHz, and $B_{\rm CMB} = 3.25(1+z)^2$ μG is the magnetic field of the cosmic microwave background. Faraday rotation measure studies indicate that magnetic field strengths in clusters are of the order of a few μG, with strengths up to tens of μG in cluster cores (e.g. Perley & Taylor 1991; Taylor & Perley 1993; Feretti et al. 1995, 1999; Taylor, Fabian & Allen 2002; Taylor et al. 2006, 2007; Bonafede et al. 2010). However, if the magnetic field in the tail has its origin in the galaxy, it would be stronger than the magnetic field in the ICM. Assuming a magnetic field strength of 10 μG, $t_{\rm syn}$ will be ∼38 Myr at 1.4 GHz for the Coma cluster ($z = 0.0231$). The mean velocity of the relativistic electrons stripped from the galaxy is about 500 km s$^{-1}$ in simulations (Tonnesen & Bryan 2010). Assuming an isotropic distribution of tail directions, the velocity in the plane of the sky is ∼400 km s$^{-1}$ (500 × $\pi/4$ km s$^{-1}$). Then, the maximum expected length of the radio continuum tail at 1.4 GHz in our observations would be 15.2 kpc, which is indeed larger than the observed length of the radio continuum tails (2.8–12.6 kpc) in the Coma cluster. The observed steepening of radio spectra in tails (especially for NGC 4858) also supports synchrotron cooling in the tail. The large uncertainty in the assumed relative velocity of the galaxy with respect to the ICM and the value for the magnetic field lead to a large range for the maximum length limitation of the radio continuum tails and the above should thus be considered to be an order of magnitude calculation based on plausible values.

### 4.1.3 *RPS galaxies without radio tails*

There are 10 galaxies without radio continuum tail detections. For 5 of them (GMP 4060, NGC 4854, GMP 3016, GMP 2923, and KUG 1258+277), no radio continuum is detected at all from the galaxy (Table 2). There is no deep H $\alpha$ data for KUG 1258+277. The H $\alpha$ tails of the other 4 (GMP 4060, NGC 4854, GMP 3016 and GMP 2923, corresponding to figs 4l, k, e, and d in Yagi et al. 2010) are weak and detached from the galaxies. At the same time, GMP 4060, GMP 3016, and GMP 2923 did not show detectable H $\alpha$ emission in the galaxies. So perhaps they are at a late evolutionary stage of stripping which might account for the weak (undetected) radio emission.

There are five galaxies (NGC 4911, NGC 4921, NGC 4853, IC 3949, and GMP 3071) with radio continuum detections in the galaxies, but radio continuum tails are not detected. NGC 4911 and NGC 4921 are both face-on galaxies. Their H $\alpha$ extensions are short, which is consistent with the lack of long radio tails there. Whereas NGC 4911 does not have a significant radio tail, its radio continuum within $D_{25}$ is asymmetric, with an extension towards the short H $\alpha$ tail. NGC 4853, IC 3949, and GMP 3071 do have significant H $\alpha$ tails, but no radio continuum tails are detected. Deeper data may be required to probe the radio continuum emission in the tails of these galaxies.

## 4.2 H I deficiency

### 4.2.1 *H I deficiency of RPS galaxies*

The RPS galaxies should be deficient in H I as it is stripped (Quilis et al. 2000; Boselli et al. 2016a). To quantify the missing atomic gas in the RPS galaxies in Coma, the H I deficiency parameter (${\rm Def}_{\rm H\,I}$, Haynes & Giovanelli 1984), or the log of the ratio of the normal (i.e. expected) H I mass and the observed H I mass, is studied with our H I results. The whole H I flux within $D_{25}$ is used to derive the ${\rm Def}_{\rm H\,I}$ for NGC 4848, NGC 4911, and IC 4040. For other galaxies, only a lower limit within $D_{25}$ can be placed on ${\rm Def}_{\rm H\,I}$. The upper limit on the H I flux is

$$S_{\rm H\,I\_ul} = 3 \times {\rm rms} \times \sqrt{W \times W_0} \times \sqrt{A_{\rm galaxy}/A_{\rm beam}}\,, \qquad (3)$$

where rms is the local noise in the H I data, in units of Jy beam$^{-1}$ channel$^{-1}$, $W$ is the expected velocity width of the galaxy in units of km s$^{-1}$, $W_0$ is the channel width of our data cube (21.5 km s$^{-1}$), $A_{\rm galaxy}$ is the $D_{25}$ area of the galaxy, and $A_{\rm beam}$ is the area of the beam size for our H I data cube. The expected velocity width of the galaxy is given by $W = 2(V_{\rm M} \sin i) + W_{\rm t}$ (Bottinelli et al. 1983), which is derived from the maximum rotational velocity ($V_{\rm M}$) by correcting the projection of inclination ($i$) and profile broadening ($W_{\rm t}$) caused by random/turbulent motions. $V_{\rm M}$ is obtained from $m_{\rm B}$ using the Tully–Fisher relation for individual galaxies (fig. 13 of Meyer et al. 2016). The values of $m_{\rm B}$ and $i$ are from LEDA and listed in Table 4. The value of $W_t$ used here is 5 km s$^{-1}$ from Verheijen & Sancisi (2001). The H I mass is given by Meyer et al. (2017):

$$M_{\rm H\,I} = \frac{2.35 \times 10^5}{(1+z)^2} \times D^2 \times S_{\rm H\,I}, \qquad (4)$$

where $M_{\rm H\,I}$ is the H I mass in M$_\odot$, $S_{\rm H\,I}$ is the H I flux in Jy km s$^{-1}$, $D$ is the luminosity distance of the galaxy in Mpc (100.7 Mpc used for all the Coma galaxies), and $z$ is the redshift of the galaxy (0.0231 used for all the Coma galaxies). The normal or expected H I mass ($M_{\rm H\,I\,normal}$) is derived based on table IV of Haynes & Giovanelli (1984), on $D_{25}$ (LEDA data base) and the galaxy type (Dressler 1980, LEDA data base). All the results are listed in Table 4.

As the H I discs of galaxies within ∼1 Mpc of the centre of clusters are typically truncated to well within the $D_{25}$ (e.g. Chung et al. 2009), our H I deficiencies should therefore be accurate. Def$_{\rm H\,I}$ for IC 4040 and the lower limits on Def$_{\rm H\,I}$ for NGC 4858, MRK 0058, NGC 4921, KUG 1258+279A, and KUG 1258+277 are consistent with Bravo-Alfaro et al. (2000) (Def$_{\rm HI\_BA00}$). However, in this work we found NGC 4848 and NGC 4911 to be less H I-deficient than Bravo-Alfaro et al. (2000). This is because the H I flux is larger than that in Bravo-Alfaro et al. (2000) which is also discussed in Section 3.3. Most (15 of 20) RPS galaxies in our sample are proved to be H I deficient with our detection and lower limit estimate. Having said that, we should keep in mind that $M_{\rm H\,I}$ could be an underestimate as any missing flux has not been considered here.

### *4.2.2 H I in the stripped tail of D100*

The mixing of the stripped cold ISM with the hot ICM will produce multiphase gas (e.g. Sun et al. 2007; Ferland et al. 2009; Jáchym et al. 2019). It is interesting to study how multiphase gases co-exist and evolve in the RPS tails. D100 is the only galaxy in our sample with CO detections in the RPS tails (Jáchym et al. 2017). With our deep and high spatial resolved H I observations, the state of co-exist molecular and atomic gas in the RPS tails of D100 could be discussed.

We were able to derive the molecular gas mass, $M_{\rm H_2}$, in the narrow tail (regions D100_T1 to D100_T4 in Jáchym et al. 2017) of D100 from CO single dish observations and Galactic standard CO–H$_2$ relation. The lower limit of $M_{\rm H_2}$ for the whole tail could be got by the sum of D100_T1 to D100_T4 as the tail is not fully covered by the CO observations. We constrain the H I mass limit in the narrow H $\alpha$ tail of D100 (∼4 arcsec width) with the new data (∼6 arcsec spatial resolution versus ∼30 arcsec spatial resolution for Bravo-Alfaro et al. 2000). The H I mass upper limit is derived using equations 2 and 3 for the whole tail (4 × 108.50 arcsec$^2$) assuming that the H I velocity width is the same as CO (the velocity coverage of CO in D100_T1 to D100_T4 is about 200 km s$^{-1}$). The H I upper limit is also derived for each part of the H $\alpha$ tail covered by CO observations (D100_T1 to D100_T4). Results are listed in Table 6. Integrated over the entire tail there is more than 5.98 × 10$^8$ M$_\odot$ of H$_2$ (assuming a Galactic CO-to-H2 conversion factor), and less than 3.51 × 10$^8$ M$_\odot$ of H I. The molecular gas fraction in (parts of) D100's stripped tail is surprisingly high, which is normally only observed in the inner disc of galaxies. This is consistent with the results in (parts of) the RPS tail of ESO137−001 (Jáchym et al. 2014).

In galaxies, the molecular to atomic gas ratio ($R_{\rm H_2}$) correlates with the interstellar pressure in the galactic disc (Blitz & Rosolowsky 2004, 2006). The ICM thermal pressure (P/k$_{\rm B}$) at the projected position of D100 (0.17 Mpc away from the cluster centroid) is 1.9 × 10$^5$ K cm$^{-3}$, which is derived from model C of the Planck Collaboration X (2013). Although the environments are completely different, the high molecular to atomic gas ratio ($R_{\rm H_2}$) and high ICM thermal pressure in (parts of) D100's stripped tail agree well with the typical relation between $R_{\rm H_2}$ and pressure in the galactic disc (fig. 9 in Krumholz, McKee & Tumlinson 2009). The high ICM thermal pressure offers an explanation for the molecular gas dominated stripped tail (Jáchym et al. 2014). On the other hand, formation of molecular gas and ionization of atomic gas in the stripped tail also increase $R_{\rm H_2}$.

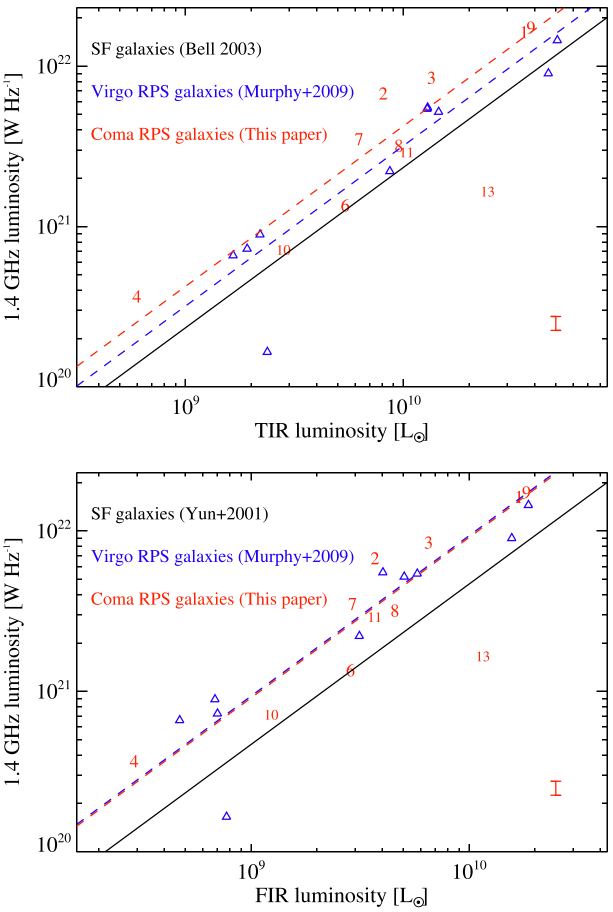

**Figure 7.** The 1.4 GHz luminosity versus TIR (top plot) and FIR (bottom plot) luminosity for the RPS galaxies. The galaxies in the Coma cluster are in red and those in the Virgo cluster (Murphy et al. 2009) are in blue. Each number indicates a galaxy as listed in Table 2. The mean ratios of 1.4 GHz to TIR (FIR) for RPS galaxies in the Coma cluster and in the Virgo cluster are shown as red and blue dashed lines, respectively. The relations between the 1.4 GHz continuum and TIR (Bell 2003) or FIR (Yun, Reddy & Condon 2001) for star-forming galaxies are also shown as black solid lines.

## 5 CONCLUSIONS

We obtained deep VLA 1.4 GHz data in two fields of the Coma cluster and focused on 20 RPS galaxies by studying their radio continuum and H I properties. Our main results are summarized as follows:

(1) Radio continuum tails are found in 10 of 20 RPS galaxies in Coma, revealing the widespread occurrence of relativistic electrons and magnetic fields in the RPS tails. 8 of the RPS tails are new detections.

(2) The wide-band 1.4 GHz data allow spectral indices to be derived which provide a hint that the radio spectra of the tails are

**Table 6.** H I in the stripped tail of D100.

| Tail region | Area_H I (arcsec$^2$) | FWHM$_{\rm CO}$ (km s$^{-1}$) | $M_{\rm H\,I}$ ($10^8$ M$_\odot$) | $M_{\rm H_2}$ ($10^8$ M$_\odot$) | $R_{\rm H2}$ | P/k$_{\rm B}$ ($10^5$ K cm$^{-3}$) |
|---|---|---|---|---|---|---|
| D100_T1 | 4 × 10.8 | 145.5 | <0.95 | $0.73 \pm 0.09$ | > 0.77 | 1.9 |
| D100_T2 | 4 × 21.7 | 165.3 | < 1.43 | $3.01 \pm 0.44$ | > 2.11 | 1.9 |
| D100_T3 | 4 × 21.7 | 52.8 | < 0.81 | $1.97 \pm 0.22$ | > 2.45 | 1.9 |
| D100_T4 | 4 × 21.7 | 31.3 | < 0.62 | $0.28 \pm 0.16$ | > 0.45 | 1.9 |
| D100_Tail | 4 × 108.5 | 200.0 | < 3.51 | > 5.98 | > 1.71 | 1.9 |

*Note.* The H I mass upper limit in the stripped tail of D100 is derived from the data presented here. The size of the H I tail is set by the H $\alpha$ emission (4 × 108.5 arcsec$^2$); the velocity width is assumed to be the same as CO (FWHM$_{\rm CO}$). D100 $M_{\rm H2}$ results adjusted to the cosmology of this paper are from CO 1–0 (Jáchym et al. 2017). The exception is the tail region of T1 where we used CO 2–1 because the beam of CO 1–0 covered part of disc. P/K$_{\rm B}$ is the ICM thermal pressure at the projected position of D100.

steeper than those of the galaxies, as expected from synchrotron cooling without injection of fresh relativistic electrons in the tails.

(3) The 1.4 GHz continuum of the stripped tails is enhanced relative to their SFR traced by H $\alpha$ emission by a factor of $\sim$7 compared to the main bodies of the galaxies. It suggests that the radio continuum in the stripped tail is not related to the local SF activity, but rather related to the ram pressure stripping.

(4) Radio emission of the RPS galaxies in the Coma cluster is also enhanced relative to its TIR (or FIR) emission by a factor of $\sim$2, compared with normal SF galaxies. Ram pressure interaction may enhance radio emission in the main bodies of the galaxies.

(5) The length of the radio continuum tails is consistent with the distance being limited by the synchrotron cooling time and stripping velocity.

(6) H I detections in three RPS galaxies (NGC 4848, NGC 4911, and IC 4040) and H I upper limits for the other galaxies are presented as well. Most (15 of 20) RPS galaxies are consistent with being deficient in H I.

(7) The H$_2$/H I mass ratio for the H $\alpha$ tail of D100 exceeds 1.6 – the cold gas in D100's stripped tail is dominated by molecular gas. This is likely a consequence of the high ICM pressure in the stripped tail.

Our continuum data imply that there are magnetic fields in the stripped tails, which could explain the collimated and bifurcated structure of the stripped gas. SF may be less efficient in a stripped tail due to suppression by magnetic fields and turbulence. We suggest that the observed radio continuum emission is due to ram pressure stripping of relativistic electrons from the host galaxy, and not so much to any local SF. This is consistent with our finding of a steeper radio spectrum in the stripped tail compared to that of the host galaxy, the overly luminous radio continuum flux density compared to the H$\alpha$, and the shorter tail length in radio (limited by the synchrotron cooling time) than in H $\alpha$. Our results also suggest that cluster late-type galaxies can inject relativistic electrons into the ICM, which could potentially feed radio relics in clusters (Ge et al. 2019).

## ACKNOWLEDGEMENTS

We acknowledge useful discussions with the NRAO help desk staff, Xing Lu, Ruoyu Liu, Neal Miller, and Stephen Walker. Support for this work was provided by NSF grant 1714764 and NASA/EPSCoR grant NNX15AK29A. We also acknowledge the support from the National Aeronautics and Space Administration through *Chandra* Award Number GO6-17111X and GO6-17127X issued by the *Chandra* X-ray Center, which is operated by the Smithsonian Astrophysical Observatory for and on behalf of the National Aeronautics Space Administration under contract NAS8-03060. HC's work has been supported by the South African Department of Science and Innovation and the National Research Foundation through a SARChI's South African SKA Fellowship within the SARAO Research Chair held by RC Kraan-Korteweg. MF has received funding from the European Research Council (ERC) under the European Union's Horizon 2020 research and innovation programme (grant agreement No 757535). This research has made use of data and/or software provided by the High Energy Astrophysics Science Archive Research Center (HEASARC), which is a service of the Astrophysics Science Division at NASA/GSFC and the High Energy Astrophysics Division of the Smithsonian Astrophysical Observatory. This research has made use of the NASA/IPAC Infrared Science Archive, which is funded by the National Aeronautics and Space Administration and operated by the California Institute of Technology. Based in part on data collected at Subaru Telescope, which is operated by the National Astronomical Observatory of Japan. We acknowledge the usage of the HyperLeda database (http://leda.univ-lyon1.fr), and the GOLDMine Database operated by the Universita' degli Studi di Milano-Bicocca, and the NASA/IPAC Extragalactic Database (NED) funded by the National Aeronautics and Space Administration and operated by the California Institute of Technology.

## DATA AVAILABILITY

Most of the data underlying this article are available in the article and in its online supplementary material. All the data will be shared on reasonable request to the corresponding authors.

## REFERENCES

Abramson A., Kenney J. D. P., 2014, AJ, 147, 63
Bell E. F., 2003, ApJ, 586, 794
Bellhouse C. et al., 2017, ApJ, 844, 49
Blitz L., Rosolowsky E., 2004, ApJ, 612, L29
Blitz L., Rosolowsky E., 2006, ApJ, 650, 933
Boissier S. et al., 2012, A&A, 545, A142
Bonafede A., Feretti L., Murgia M., Govoni F., Giovannini G., Dallacasa D., Dolag K., Taylor G. B., 2010, A&A, 513, A30
Boselli A. et al., 2016a, A&A, 587, A68
Boselli A. et al., 2016b, A&A, 596, A11
Boselli A. et al., 2018, A&A, 615, A114
Bottinelli L., Gouguenheim L., Paturel G., de Vaucouleurs G., 1983, A&A, 118, 4
Bravo-Alfaro H., Cayatte V., van Gorkom J. H., Balkowski C., 2000, AJ, 119, 580
Bravo-Alfaro H., Cayatte V., van Gorkom J. H., Balkowski C., 2001, A&A, 379, 347
Butler A. et al., 2018, A&A, 620, A16
Chung A., van Gorkom J. H., Kenney J. D. P., Crowl H., Vollmer B., 2009, AJ, 138, 1741

Chung A., van Gorkom J. H., Kenney J. D. P., Vollmer B., 2007, ApJ, 659, L115

Condon J. J., Anderson M. L., Helou G., 1991, ApJ, 376, 95

Condon J. J., Cotton W. D., Greisen E. W., Yin Q. F., Perley R. A., Taylor G. B., Broderick J. J., 1998, AJ, 115, 1693

Cortese L., Gavazzi G., Boselli A., Iglesias-Paramo J., 2004, A&A, 416, 119

Cortese L. et al., 2007, MNRAS, 376, 157

Cramer W. J., Kenney J. D. P., Sun M., Crowl H., Yagi M., Jáchym P., Roediger E., Waldron W., 2019, ApJ, 870, 63

Crowl H. H., Kenney J. D., van Gorkom J. H., Chung A., Rose J. A., 2006, American Astronomical Society Meeting Abstracts. p. 211.11

Crowl H. H., Kenney J. D. P., van Gorkom J. H., Vollmer B., 2005, AJ, 130, 65

Deb T. et al., 2020, MNRAS, 494, 5029

Dressler A., 1980, ApJS, 42, 565

Ebeling H., Stephenson L. N., Edge A. C., 2014, ApJ, 781, L40

Feretti L., Dallacasa D., Giovannini G., Tagliani A., 1995, A&A, 302, 680

Feretti L., Dallacasa D., Govoni F., Giovannini G., Taylor G. B., Klein U., 1999, A&A, 344, 472

Feretti L., Giovannini G., 2008, in Plionis M., López-Cruz O., Hughes D., eds, Lecture Notes in Physics, Vol. 740, A Pan-Chromatic View of Clusters of Galaxies and the Large-Scale Structure. Springer-Verlag, Berlin, p. 24

Ferland G. J., Fabian A. C., Hatch N. A., Johnstone R. M., Porter R. L., van Hoof P. A. M., Williams R. J. R., 2009, MNRAS, 392, 1475

Fossati M., Fumagalli M., Boselli A., Gavazzi G., Sun M., Wilman D. J., 2016, MNRAS, 455, 2028

Fossati M., Gavazzi G., Boselli A., Fumagalli M., 2012, A&A, 544, A128

Fossati M. et al., 2018, A&A, 614, A57

Fumagalli M., Fossati M., Hau G. K. T., Gavazzi G., Bower R., Sun M., Boselli A., 2014, MNRAS, 445, 4335

Galametz M. et al., 2013, MNRAS, 431, 1956

Gavazzi G., , Boselli A., Donati A., Franzetti P., Scodeggio M., 2003, A&A, 400:451

Gavazzi G., 1978, A&A, 69, 355

Gavazzi G., Boselli A., Kennicutt R., 1991, AJ, 101, 1207

Gavazzi G., Boselli A., Mayer L., Iglesias-Paramo J., Vílchez J. M., Carrasco L., 2001, ApJ, 563, L23

Gavazzi G., Consolandi G., Gutierrez M. L., Boselli A., Yoshida M., 2018, A&A, 618, A130

Gavazzi G., Consolandi G., Yagi M., Yoshida M., 2017, A&A, 606, A131

Gavazzi G., Contursi A., Carrasco L., Boselli A., Kennicutt R., Scodeggio M., Jaffe W., 1995, A&A, 304, 325

Gavazzi G., Jaffe W., 1985, ApJ, 294, L89

Gavazzi G., Jaffe W., 1986, ApJ, 310, 53

Gavazzi G., Jaffe W., 1987, A&A, 186, L1

Ge C. et al., 2019, MNRAS, 486, L36

Gerhard O., Arnaboldi M., Freeman K. C., Okamura S., 2002, ApJ, 580, L121

Gunn J. E., Gott J. R., 1972, ApJ, 176, 1

Haynes M. P., Giovanelli R., 1984, AJ, 89, 758

Helou G., Soifer B. T., Rowan-Robinson M., 1985, ApJ, 298, L7

Jáchym P., Combes F., Cortese L., Sun M., Kenney J. D. P., 2014, ApJ, 792, 11

Jáchym P., Kenney J. D. P., Ržuička A., Sun M., Combes F., Palouš J., 2013, A&A, 556, A99

Jáchym P. et al., 2017, ApJ, 839, 114

Jáchym P. et al., 2019, ApJ, 883, 145

Kang H., Ryu D., 2011, ApJ, 734, 18

Kapferer W., Sluka C., Schindler S., Ferrari C., Ziegler B., 2009, A&A, 499, 87

Kenney J. D. P., Abramson A., Bravo-Alfaro H., 2015, AJ, 150, 59

Kenney J. D. P., Geha M., Jáchym P., Crowl H. H., Dague W., Chung A., van Gorkom J., Vollmer B., 2014, ApJ, 780, 119

Kenney J. D. P., van Gorkom J. H., Vollmer B., 2004, AJ, 127, 3361

Kim K.-T., 1994, A&AS, 105, 403

Koda J., Yagi M., Yamanoi H., Komiyama Y., 2015, ApJ, 807, L2

Koopmann R. A., Kenney J. D. P., 2004, ApJ, 613, 866

Krumholz M. R., McKee C. F., Tumlinson J., 2009, ApJ, 693, 216

Makarov D., Prugniel P., Terekhova N., Courtois H., Vauglin I., 2014, A&A, 570, A13

Meyer M., Robotham A., Obreschkow D., Westmeier T., Duffy A. R., Staveley-Smith L., 2017, Publ. Astron. Soc. Aust., 34, 52

Meyer S. A., Meyer M., Obreschkow D., Staveley-Smith L., 2016, MNRAS, 455, 3136

Miller N. A., Hornschemeier A. E., Mobasher B., 2009, AJ, 137, 4436

Mohan N., Rafferty D., 2015, Astrophysics Source Code Library, record ascl:1502.007

Moretti A. et al., 2018, MNRAS, 480, 2508

Murphy E. J., Helou G., Kenney J. D. P., Armus L., Braun R., 2008, ApJ, 678, 828

Murphy E. J., Kenney J. D. P., Helou G., Chung A., Howell J. H., 2009, ApJ, 694, 1435

Nulsen P. E. J., 1982, MNRAS, 198, 1007

Oosterloo T., van Gorkom J., 2005, A&A, 437, L19

Owers M. S., Couch W. J., Nulsen P. E. J., Randall S. W., 2012, ApJ, 750, L23

Perley R. A., Taylor G. B., 1991, AJ, 101, 1623

Pinzke A., Oh S. P., Pfrommer C., 2013, MNRAS, 435, 1061

Planck Collaboration X, 2013, A&A, 554, A140

Poggianti B. M. et al., 2016, AJ, 151, 78

Poggianti B. M. et al., 2017, ApJ, 844, 48

Quilis V., Moore B., Bower R., 2000, Science, 288, 1617

Ramatsoku M. et al., 2019, MNRAS, 487, 4580

Roediger E., Bruggen M., Owers M. S., Ebeling H., Sun M., 2014, MNRAS, 443, L114

Roediger E., Brüggen M., 2008, MNRAS, 388, 465

Ruszkowski M., 2012, The Role of Magnetic Fields and Microphysics in Ram Pressure Stripping, NASA Proposal id.12-ATP12-17

Sanders J. S., Fabian A. C., Sun M., Churazov E., Simionescu A., Walker S. A., Werner N., 2014, MNRAS, 439, 1182

Scott T. C., Cortese L., Brinks E., Bravo-Alfaro H., Auld R., Minchin R., 2012, MNRAS, 419, L19

Scott T. C., Usero A., Brinks E., Boselli A., Cortese L., Bravo-Alfaro H., 2013, MNRAS, 429, 221

Scott T. C., Usero A., Brinks E., Bravo-Alfaro H., Cortese L., Boselli A., Argudo-Fernández M., 2015, MNRAS, 453, 328

Scott T. C. et al., 2010, MNRAS, 403, 1175

Serra P. et al., 2015, MNRAS, 448, 1922

Serra P. et al., 2019, A&A, 628, A122

Sivanandam S., Rieke M. J., Rieke G. H., 2010, ApJ, 717, 147

Sivanandam S., Rieke M. J., Rieke G. H., 2014, ApJ, 796, 89

Smith R. J. et al., 2010, MNRAS, 408, 1417

Smolčić V. et al., 2017, A&A, 602, A1

Snowden S. L., Mushotzky R. F., Kuntz K. D., Davis D. S., 2008, A&A, 478, 615

Struble M. F., 2018, MNRAS, 473, 4686

Sun M., Donahue M., Roediger E., Nulsen P. E. J., Voit G. M., Sarazin C., Forman W., Jones C., 2010, ApJ, 708, 946

Sun M., Donahue M., Voit G. M., 2007, ApJ, 671, 190

Sun M., Jones C., Forman W., Nulsen P. E. J., Donahue M., Voit G. M., 2006, ApJ, 637, L81

Taylor G. B., Fabian A. C., Allen S. W., 2002, MNRAS, 334, 769

Taylor G. B., Fabian A. C., Gentile G., Allen S. W., Crawford C., Sanders J. S., 2007, MNRAS, 382, 67

Taylor G. B., Gugliucci N. E., Fabian A. C., Sanders J. S., Gentile G., Allen S. W., 2006, MNRAS, 368, 1500

Taylor G. B., Perley R. A., 1993, ApJ, 416, 554

Tonnesen S., Bryan G. L., 2010, ApJ, 709, 1203

Tonnesen S., Bryan G. L., 2012, MNRAS, 422, 1609

Tonnesen S., Bryan G. L., Chen R., 2011, ApJ, 731, 98

Valentijn E. A., Perola G. C., Jaffe W. J., 1977, A&AS, 28, 333

Verdugo C., Combes F., Dasyra K., Salomé P., Braine J., 2015, A&A, 582, A6

Verheijen M. A. W., Sancisi R., 2001, A&A, 370, 765

Vollmer B., Beck R., Kenney J. D. P., van Gorkom J. H., 2004, AJ, 127, 3375

Vollmer B., Soida M., Beck R., Chung A., Urbanik M., Chyży K. T., Otmianowska-Mazur K., Kenney J. D. P., 2013, A&A, 553, A116
White R. L., Becker R. H., Helfand D. J., Gregg M. D., 1997, ApJ, 475, 479
Wold I. G. B., Owen F. N., Wang W.-H., Barger A. J., Keenan R. C., 2012, ApJS, 202, 2
Yagi M., Gu L., Fujita Y., Nakazawa K., Akahori T., Hattori T., Yoshida M., Makishima K., 2013, ApJ, 778, 91
Yagi M., Koda J., Komiyama Y., Yamanoi H., 2016, ApJS, 225, 11
Yagi M., Komiyama Y., Yoshida M., Furusawa H., Kashikawa N., Koyama Y., Okamura S., 2007, ApJ, 660, 1209
Yagi M., Yoshida M., Gavazzi G., Komiyama Y., Kashikawa N., Okamura S., 2017, ApJ, 839, 65
Yagi M. et al., 2010, AJ, 140, 1814
Yoshida M., Yagi M., Komiyama Y., Furusawa H., Kashikawa N., Hattori T., Okamura S., 2012, ApJ, 749, 43
Yoshida M. et al., 2008, ApJ, 688, 918
Yun M. S., Reddy N. A., Condon J. J., 2001, ApJ, 554, 803
Zhang B. et al., 2013, ApJ, 777, 122

## SUPPORTING INFORMATION

Supplementary data are available at *MNRAS* online.

**Table B1.** The full continuum source catalogue.

## APPENDIX A: RADIO CONTINUUM MAP

A mosaic image of our radio continuum observations is shown in Fig. A1. It is the combination of the 30 per cent response regions of the two fields. Magnified images of two sources are shown at the right to show them in detail. The narrow tail near the end of NGC 4869 is shown better in our image than in Miller et al. (2009). The source in the lower right panel (the small dashed line box on the left) has an interesting complex structure that is not covered by Miller et al. (2009). This source is catalogued as 1254+28W07 (Valentijn, Perola & Jaffe 1977; Kim 1994) and NVSS J125720+282727 (Condon et al. 1998), but the complex structure is not resolved because of the low spatial resolution (>45 arcsec).

## APPENDIX B: FLUX DENSITY MEASUREMENTS

The full continuum source catalogue is shown in Table B1. As Fig. B1 shows, our deep observations reveal many more continuum sources than Miller et al. (2009). To assess the reliability of the flux density measurement of our work, we compared our results with Miller et al. (2009) and the FIRST survey (White et al. 1997). Because the spatial resolution is about 5 arcsec, we cross-match Miller's and FIRST sources with ours for match radii of 5 arcsec. Sources are excluded when more than one match is found within 5 arcsec. The comparisons are shown in Fig. B2. Our flux density measurements are consistent with those from Miller et al. (2009) and FIRST. There is still some scatter, which could be caused by: (1) different algorithms

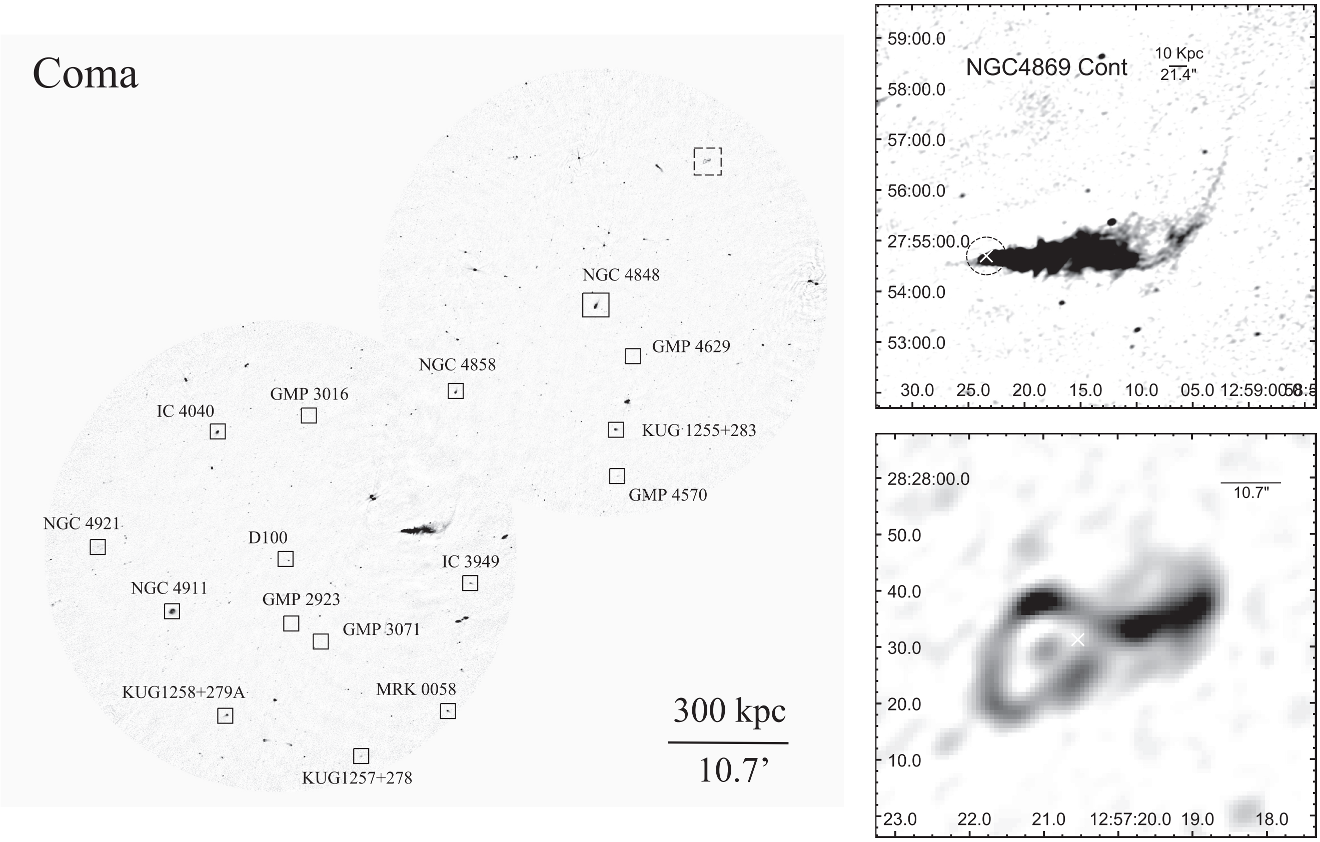

**Figure A1.** Left: Radio continuum image of two fields in the Coma cluster (30 per cent response shown here). The galaxies shown in Fig. 1 and also covered by 30 per cent response are marked as solid squares. Right: zoom-in radio continuum images of two interesting sources: the narrow-angle tailed galaxy NGC 4869, and an interesting source at 12:57:20.54 +28:27:31.28 (J2000.0) marked as a dashed square.

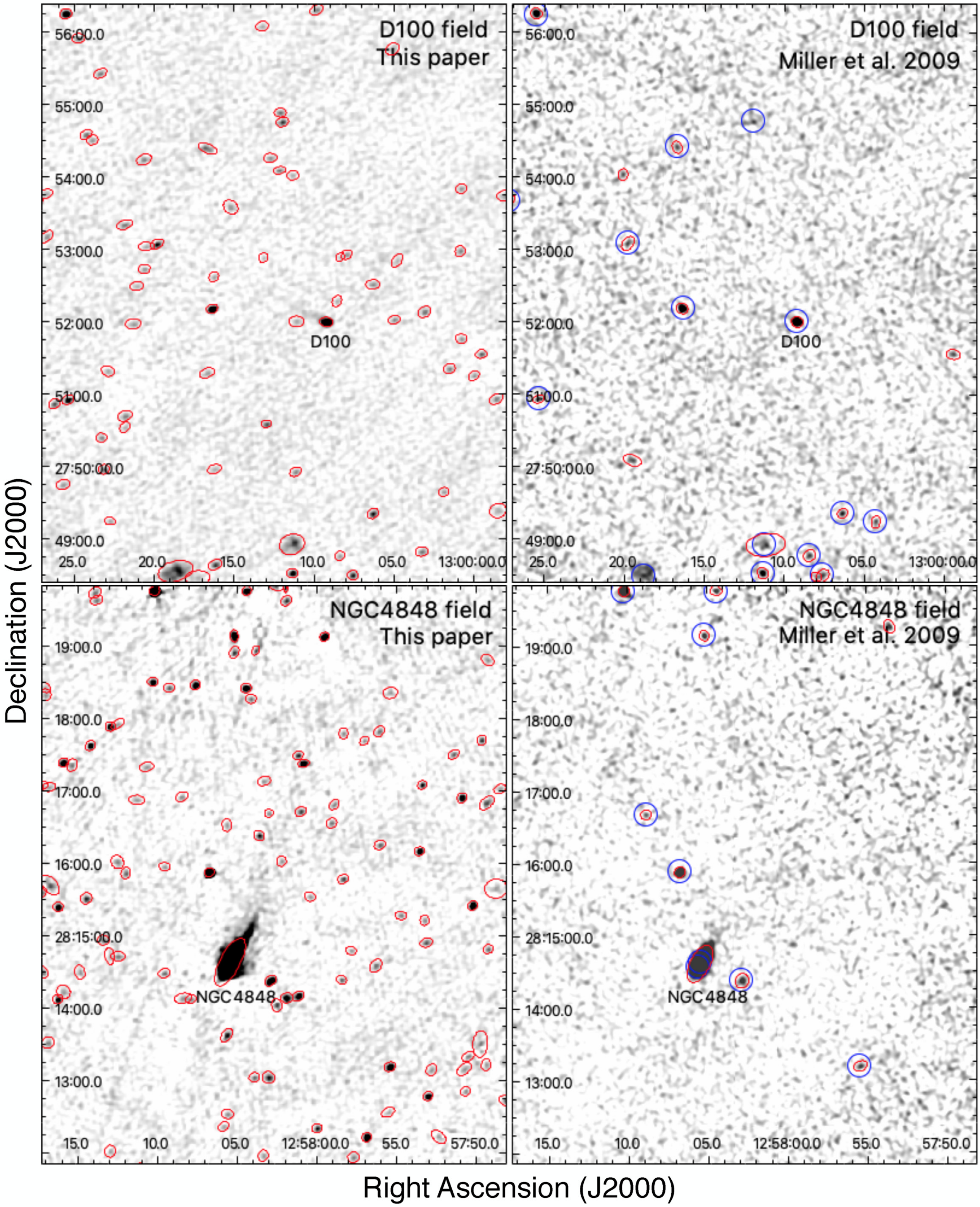

**Figure B1.** Comparison of sources detected with PYBDSF between this work and Miller et al. (2009). Red apertures show the radio continuum sources defined with PYBDSF. Blue circles show the sources detected by Miller et al. (2009) (the radii are fixed at 20 arcsec).

**Table B1.** The full continuum source catalogue.

| ID (1) | RA (J2000) (2) (h m s) | Dec. (J2000) (3) (° ′ ″) | $S_{\rm int}$ (4) (μJy) | $\Delta S_{\rm int}$ (5) (μJy) | Field (6) |
|---|---|---|---|---|---|
| 1 | 12 56 2.35 | 28 15 28.6 | 181 | 60 | 1 |
| 2 | 12 56 2.73 | 28 13 15.6 | 141 | 57 | 1 |
| 3 | 12 56 2.77 | 28 15 24.6 | 169 | 93 | 1 |
| 4 | 12 56 3.68 | 28 15 49.9 | 217 | 72 | 1 |
| 5 | 12 56 3.69 | 28 20 52.4 | 123 | 47 | 1 |

*Note.* Column descriptions: (1) source ID; (2) and (3) right ascension and declination (J2000) of radio source peak; (4) and (5) integral flux density and its associated error at 1.4 GHz; (6) The field (shown in Fig. 1 and Table 1) in which source was found. For the 64 sources covered by both fields, their results from the two fields are listed in different rows, respectively, and the same source ID was set for the same source. (This table is available in its entirety in machine-readable form online. A portion is shown here for guidance regarding its form and content.)

of source detection (PYBDSF in our work and SAD in Miller et al. 2009 and FIRST); and/or (2) varying radio sources (e.g. AGNs). We also applied the PYBDSF algorithms to the data of Miller et al. (2009) to compare the flux density measurements. By applying PYBDSF on both our data and the Miller et al. (2009) data, the consistency on the flux density measurements is improved, with the root-mean-squared error of the fits decreasing from 3.0 to 1.3 mJy. Linear fits of comparison show that: $S_{\rm Miller+2009}[\rm mJy] = (1.07 \pm 0.11) \times S_{\rm Ours}[\rm mJy]$ $S_{\rm FIRST}[\rm mJy] = (0.94 \pm 0.23) \times S_{\rm Ours}[\rm mJy]$

$S_{\rm Miller+2009}[\rm mJy] = (0.95 \pm 0.09) \times S_{\rm PyBDSF\,Miller}[\rm mJy]$

Power-law fits confirm the linear relations between our flux density and the Miller et al. (2009) flux density (an index of 1.00 ± 0.07), and the FIRST flux density (an index of 1.00 ± 0.06).

## APPENDIX C: 1.4 GHZ CONTINUUM SOURCE COUNTS

Our new data generated the largest 1.4 GHz source catalogue in the Coma cluster. We compare source counts in our regions with those from previous work in Fig. C1. The source count is defined as $S^{2.5}{\rm d}N/{\rm d}S/A$. $S$ is the source flux density, $N$ is the source number, and $A$ is the observed sky area in steradians. Our source count is restricted to the 1975 and 1173 sources identified by PYBDSF in two fields. The sky area, $A$, is different for each bin of flux density, $S$. For flux density $S$, we used the sky area for which the rms was less than 1/4 $S$, because only sources with a peak flux density greater than 4$\sigma$ are identified by PYBDSF. In both fields, the rms increases with the distance from the centre because of the primary beam correction. So the region that is sensitive enough to detect faint sources is smaller than the region to detect bright sources. The uncertainties in source counts were derived from Poisson statistics. Our results are consistent with other studies between 0.1 and 110 mJy. For lower flux density, the source counts are lower than Smolčić et al. (2017). However, we need to keep in mind that the completeness and bias corrections used by Smolčić et al. (2017) have not been applied to our data. The correction could be as large as a factor of 3 for a source with a flux density of 5$\sigma$ (Table 4 and fig. 18 of Smolčić et al. 2017). At the same time, some inconsistency could be caused by different software packages (e.g. PYBDSF in our work, BLOBCAT in Smolčić et al. 2017 and Butler et al. 2018, and SAD in Miller et al. 2009 and Wold et al. 2012) and thresholds (source peaks greater than S/N > 4 or S/N > 5) used to identify sources in these studies.

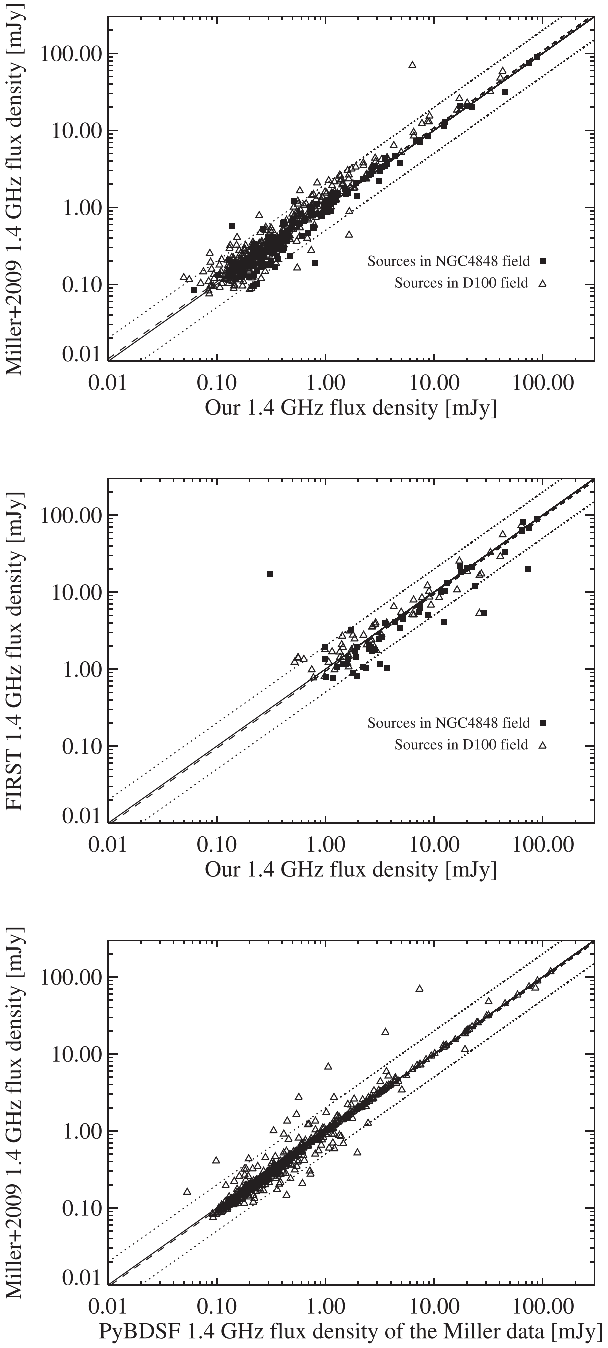

**Figure B2.** Top two plots show the flux density comparison between this work and Miller et al. (2009) and the FIRST survey (White et al. 1997). The bottom plot shows the comparison between Miller et al. (2009) and PYBDSF results on their data. Dotted lines show an uncertainty of 0.3 index, while dashed and solid lines show the linear and power-law fitting results.

## APPENDIX D: RADIO EMISSION FROM ULTRA-DIFFUSE GALAXIES IN THE COMA CLUSTER

We also examined the radio emission from ultra-diffuse galaxies (UDGs) in the Coma cluster. With the radio sources detected in Miller et al. (2009), Struble (2018) found no evidence for radio emission from UDGs. We match the 3084 radio sources detected

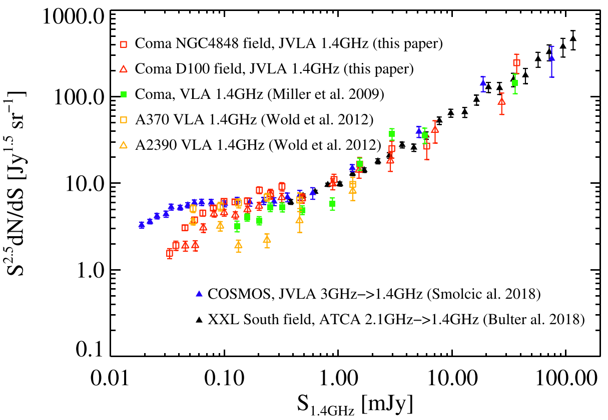

**Figure C1.** Comparison of source counts from our work and previous results. For comparison, 3 and 2.1 GHz flux densities from Smolčić et al. (2017) and Butler et al. (2018) are converted to 1.4 GHz flux densities assuming a spectral index of −0.7 and −0.75, respectively.

in our deep observations and the UDGs in the Coma cluster (Koda et al. 2015; Yagi et al. 2016). There are 449 UDGs within our fields (field 1 + 2, out to the 10 per cent primary beam response level) that cover 4152.9 arcmin$^2$. We find that there is 1 match within a 2 arcsec radius, 6 matches within a 5 arcsec radius, and 26 matches within a 10 arcsec radius. Following Struble (2018), the expected number of random matches within an offset of $r$ is ∼1.2 for $r < 2$ arcsec, ∼7.3 for $r < 5$ arcsec, and ∼29.0 for $r < 10$ arcsec. Thus, even with our much deeper radio data, there is no evidence of radio emission from UDGs in the Coma cluster.

[1] *Department of Physics & Astronomy, University of Alabama in Huntsville, 301 Sparkman Drive, Huntsville, AL 35899, USA*

[2] *Department of Astronomy, University of Cape Town, Private Bag X3, Rondebosch 7701, South Africa*

[3] *Optical and Infrared Astronomy Division, National Astronomical Observatory of Japan, Mitaka, Tokyo 181-8588, Japan*

[4] *Graduate School of Science and Engineering, Hosei University, 3-7-2, Kajinocho, Koganei, Tokyo 184-8584, Japan*

[5] *Departamento de Astronomía, Universidad de Guanajuato, Apdo. Postal 144, Guanajuato 36000, Mexico*

[6] *Centre for Astrophysics Research, University of Hertfordshire, College Lane, Hatfield AL10 9AB, UK*

[7] *Astronomy Department, Yale University, P.O. Box 208101, New Haven, CT 06520-8101, USA*

[8] *Observatoire de Paris, LERMA, College de France, CNRS, PSL Univ, Sorbonne University, UPMC, F-75014 Paris, France*

[9] *Department of Astronomy and Astrophysics, University of Toronto, 50 St. George St, Toronto, ON M5S 3H4, Canada*

[10] *Dunlap Institute for Astronomy and Astrophysics, University of Toronto, 50 St. George St, Toronto, ON M5S 3H4, Canada*

[11] *Astronomical Institute, Academy of Sciences of the Czech Republic, Boční II 1401, CZ-141 31 Prague 4, Czech Republic*

[12] *Dipartimento di Fisica G. Occhialini, Universitä degli Studi di Milano Bicocca, Piazza della Scienza 3, I-20126 Milano, Italy*

[13] *Institute for Computational Cosmology and Center for Extragalactic Astronomy, Durham University, South Road, Durham DH1 3LE, UK*

[14] *Università degli Studi di Milano-Bicocca, Piazza della Scienza 3, I-20126 Milano, Italy*

[15] *Aix Marseille Univ, CNRS, CNES, LAM, UMR 7326, F-13388, Marseille, France*

[16] *Harvard–Smithsonian Center for Astrophysics, 60 Garden Street, Cambridge, MA 02138, USA*

[17] *ICRAR, University of Western Australia, 35 Stirling Hwy, Crawley, WA 6009, Australia*

[18] *Department of Astronomy, University of Virginia, Charlottesville, VA 22904, USA*

[19] *Subaru Telescope, National Astronomical Observatory of Japan, 650 North A'ohoku Place, Hilo, HI 96720, USA*

[20] *Hiroshima Astrophysical Science Center, Hiroshima University, Higashi-Hiroshima, Hiroshima 739-8526, Japan*

[21] *Milne Centre for Astrophysics, Department of Physics & Mathematics, University of Hull, Hull HU6 7RX, UK*

This paper has been typeset from a TEX/LATEX file prepared by the author.